

# 1 **Implementation of trait-based ozone plant sensitivity in the Yale** 2 **Interactive terrestrial Biosphere model v1.0 to assess global vegetation** 3 **damage**

4  
5 **Yimian Ma**<sup>1,2</sup>, **Xu Yue**<sup>3\*</sup>, **Stephen Sitch**<sup>4\*</sup>, **Nadine Unger**<sup>3</sup>, **Johan Uddling**<sup>5</sup>, **Lina M. Mercado**<sup>4,6</sup>,  
6 **Cheng Gong**<sup>7</sup>, **Zhaozhong Feng**<sup>8</sup>, **Huiyi Yang**<sup>9</sup>, **Hao Zhou**<sup>1,2</sup>, **Chenguang Tian**<sup>1,2</sup>, **Yang Cao**<sup>1,2</sup>,  
7 **Yadong Lei**<sup>10</sup>, **Alexander W. Cheesman**<sup>4,11</sup>, **Yansen Xu**<sup>8</sup>, **Maria Carolina Duran Rojas**<sup>12</sup>

8  
9  
10 <sup>1</sup> Climate Change Research Center, Institute of Atmospheric Physics, Chinese Academy of Sciences,  
11 Beijing, 100029, China

12 <sup>2</sup> University of Chinese Academy of Sciences, Beijing, 100029, China

13 <sup>3</sup> Jiangsu Key Laboratory of Atmospheric Environment Monitoring and Pollution Control, Jiangsu  
14 Collaborative Innovation Center of Atmospheric Environment and Equipment Technology, School of  
15 Environmental Science and Engineering, Nanjing University of Information Science and Technology,  
16 Nanjing, 210044, China

17 <sup>4</sup> Faculty of Environment, Science and Economy, University of Exeter, Exeter, EX4 4RJ, UK

18 <sup>5</sup> Department of Biological and Environmental Sciences, University of Gothenburg, Gothenburg, P.O.  
19 Box 461, 40530, Sweden

20 <sup>6</sup> UK Centre for Ecology and Hydrology, Benson Lane, Wallingford, OX10 8BB, UK

21 <sup>7</sup> State Key Laboratory of Atmospheric Boundary Layer Physics and Atmospheric Chemistry (LAPC),  
22 Institute of Atmospheric Physics, Chinese Academy of Sciences, Beijing, 100029, China

23 <sup>8</sup> School of Applied Meteorology, Nanjing University of Information Science and Technology, Nanjing,  
24 210044, China

25 <sup>9</sup> Livelihoods and Institutions Department, Natural Resources Institute, University of Greenwich, Kent,  
26 ME4 4TB, UK

27 <sup>10</sup> Chinese Academy of Meteorological Sciences, Beijing, 100081, China

28 <sup>11</sup> Centre for Tropical Environmental and Sustainability Science, College of Science & Engineering,  
29 James Cook University, Cairns, Queensland, 4870 Australia

30 <sup>12</sup> College of Engineering, Mathematics, and Physical Sciences, University of Exeter, Exeter, EX4 4PY,  
31 UK

32  
33 *Correspondence to:* Xu Yue ([yuexu@nuist.edu.cn](mailto:yuexu@nuist.edu.cn)) and Stephen Sitch ([S.A.Sitch@exeter.ac.uk](mailto:S.A.Sitch@exeter.ac.uk))

34

35

36

37

## Abstract

38

39 A major limitation in modeling global ozone ( $O_3$ ) vegetation damage has long been the reliance on  
40 empirical  $O_3$  sensitivity parameters derived from a limited number of species and applied at the level of  
41 plant functional types (PFTs), which ignore the large interspecific variations within the same PFT. Here,  
42 we present a major advance in large-scale assessments of  $O_3$  plant injury by linking the trait leaf mass per  
43 area (LMA) and plant  $O_3$  sensitivity in a broad and global perspective. Application of the new approach  
44 and a global LMA map in a dynamic global vegetation model reasonably represents the observed  
45 interspecific responses to  $O_3$  with a unified sensitivity parameter for all plant species. Simulations suggest  
46 a contemporary global mean reduction of 4.8% in gross primary productivity by  $O_3$ , with a range of 1.1%-  
47 12.6% for varied PFTs. Hotspots with damages  $> 10\%$  are found in agricultural areas in the eastern U.S.,  
48 western Europe, eastern China, and India, accompanied by moderate to high levels of surface  $O_3$ .  
49 Furthermore, we simulate the distribution of plant sensitivity to  $O_3$ , which is highly linked with the  
50 inherent leaf trait trade-off strategies of plants, revealing high risks for fast-growing species with low  
51 LMA, such as crops, grasses and deciduous trees.

52

## 53 **1. Introduction**

54 Tropospheric ozone (O<sub>3</sub>) has long been recognized as a hazardous pollutant for plants (Richards et al.,  
55 1958; Reich and Amundson, 1985; Richards et al., 1958). ~~As a strong oxidant, O<sub>3</sub> can cause damage to~~  
56 ~~leaf cells and modulate the carbon balance of ecosystems through both direct and indirect impacts on~~  
57 ~~plant function (Ainsworth et al., 2012; Feng et al., 2014; Wittig et al., 2009).~~ To date, O<sub>3</sub> fumigation  
58 ~~experiments have revealed a large variation in O<sub>3</sub> sensitivities among and within plant functional types~~  
59 ~~(PFTs).~~ As a strong oxidant, O<sub>3</sub> can cause damage to leaf cells (Feng et al., 2014), impact stomata  
60 conductance (Buker et al., 2015; Mills et al., 2018a), and reduce photosynthesis and biomass (Wittig et  
61 al., 2009). These negative impacts dampen global plant productivity (Ainsworth et al., 2012; Ainsworth  
62 et al., 2020) and crop yield (Tai et al., 2014; Emberson et al., 2018; Feng et al., 2022), altering multiple  
63 ecosystem functions and services across various spatiotemporal scales (Agathokleous et al., 2020; Feng  
64 et al., 2021). Thus, it is of crucial importance to quantify O<sub>3</sub> plant damage in global modeling and assess  
65 its coupling effects in the biosphere-atmosphere systems (Zhou et al., 2018).

66

67 To date, O<sub>3</sub> fumigation experiments have been conducted for various plant species. Accordingly, O<sub>3</sub>  
68 damaging sensitivities, denoted as the Dose-Response Relationships (DRRs), were derived as the  
69 regressions between O<sub>3</sub> exposure metrics and the changes in biotic indicators (Mills et al., 2011). The  
70 widely-used O<sub>3</sub> metrics include ambient O<sub>3</sub> concentrations for AOT40 (Accumulated O<sub>3</sub> concentration  
71 above the Threshold of 40 ppbv (Fuhrer et al., 1997)), or the stomatal O<sub>3</sub> flux for POD<sub>y</sub> (Phytotoxic O<sub>3</sub>  
72 Dose above a threshold flux of y (Buker et al., 2015)). The biotic indicators include visual leaf states,  
73 photosynthetic rate, biomass, or crop yield. Normally, the DRRs were derived for typical tree/grass  
74 species at specific regions, for example, Norway spruce, birch, and beech in Europe (Buker et al., 2015)  
75 or poplar (Shang et al., 2017) and crops (Peng et al., 2019) in East Asia.

76

77 Some assessment studies used DRRs to derive contemporary O<sub>3</sub> plant damage patterns at large scales.  
78 Concentration-based DRRs were widely measured and applied on the homogenized land cover, mostly  
79 for estimating crop yield loss (Feng et al., 2022; Tai et al., 2021; Hong et al., 2020). However, such DRRs  
80 don't include information about biochemical defense and stomatal regulations. Comparatively, flux-based

81 DRRs reflect a more reasonable consideration in biological processes, but are limited by the application  
82 scales in both space and time (Mills et al., 2011; Mills et al., 2018b). For example, the estimate of  $POD_y$   
83 needs a dry deposition model “ $DO_3SE$ ” (Deposition of Ozone for Stomatal Exchange) (Clrtap, 2017) or  
84 an equivalent model to account for environmental constraints on plant stomatal uptake during the whole  
85 growing season. Furthermore, the application of DRRs might introduce uncertainties due to the omission  
86 of complex interactions among biotic and abiotic factors at varied spatiotemporal scales.

87

88 Alternatively, more and more mechanistic schemes were developed and implemented in dynamic global  
89 vegetation models (DGVMs) to assess the joint effects of environmental factors and  $O_3$  on plants. Felzer  
90 et al. (2004) considered both the damaging (through AOT40) and healing (through growth) processes  
91 related to  $O_3$  effects within the framework of Terrestrial Ecosystem Model. They further estimated the  
92 reduction of 2.6%-6.8% in the net primary productivity by  $O_3$  pollution in U.S. during 1980-1990.  
93 Different from Felzer et al. (2004), Sitch et al. (2007) proposed a flux-based scheme linking the  
94 instantaneous  $POD_y$  with the damaging percentage through the coupling between stomatal conductance  
95 and photosynthetic rate. Implementing this scheme into the vegetation model of YIBs, Yue and Unger  
96 (2015) predicted a range of 2%-5% reduction in global gross primary productivity (GPP) taking into  
97 account the low to high  $O_3$  sensitivities for each vegetation types. Lombardozzi et al. (2015) collected  
98 hundreds of measurements and derived the decoupled responses in stomatal conductance and  
99 photosynthesis for the same  $O_3$  uptake fluxes. They further implemented the separate response  
100 relationships into the Community Land Model and estimated a reduction of 8%-12% in GPP by  $O_3$  at  
101 present day. Coupling these schemes with earth system models, studies have assessed interactive  $O_3$   
102 impacts on carbon sink (Oliver et al., 2018; Yue and Unger, 2018), global warming (Sitch et al., 2007),  
103 and air pollution (Zhou et al., 2018; Gong et al., 2020; Gong et al., 2021; Zhu et al., 2022).

104

105 Although different schemes considered varied physical processes (Ollinger et al., 1997; Felzer et al., 2004;  
106 Sitch et al., 2007; Felzer et al., 2009; Lombardozzi et al., 2015; Oliver et al., 2018), they followed the  
107 same principle that different  $O_3$  sensitivities should be applied for varied plant functional types (PFTs),  
108 as revealed by many measurements in the past four decades (Buker et al., 2015; Mills et al., 2018b) (Table



109 S1). Generally, needleleaf trees, deciduous woody plants, and crop species show ascending sensitivities  
110 to O<sub>3</sub> (~~Baker et al., 2015~~ Reich and Amundson, 1985; Davison and Barnes, 1998; ~~Reich and Amundson,~~  
111 ~~1985~~ ~~Baker et al., 2015~~). ~~The~~ ~~But the~~ cause of such variation is not fully understood and thus has not been  
112 uniformly described in vegetation models (Massman et al., 2000; Tiwari et al., 2016). As a result, all  
113 large-scale assessments of O<sub>3</sub> vegetation damage have had to rely on a PFT-based range of sensitivity  
114 parameters derived from a limited number of plant species (~~Felzer et al., 2009; Lombardozzi et al., 2015;~~  
115 ~~Sitch et al., 2007~~). ~~For example, Sitch et al. (2007) (hereafter S2007) and~~ attempted to envelop the range  
116 of O<sub>3</sub> impacts by assuming all species within a PFT are either “high” or “low” sensitive to O<sub>3</sub>, ~~which~~  
117 ~~cannot resolve intra-PFT variations.~~ For example, Felzer et al. (2004) defined empirical sensitivity  
118 coefficients for three major plants including deciduous trees, coniferous trees, and crops. In Sitch et al.  
119 (2007), the sensitivity coefficients were defined separately for five PFTs with high/low ranges calibrated  
120 by DRRs of typical species. These synthesized assumptions cannot resolve the intra-PFT variations in the  
121 O<sub>3</sub> sensitivity and thus may cause large uncertainties in regional to global assessments.

122  
123 Recent observations revealed a uniform plant sensitivity to O<sub>3</sub> if stomatal O<sub>3</sub> flux ~~is was~~ expressed based  
124 on leaf mass rather than leaf area (Li et al., 2016; Feng et al., 2018; Li et al., ~~2016~~; ~~Li et al., 2022~~). The  
125 trait of leaf mass per area (LMA) is an important metric linking leaf area to mass. In a comparative study  
126 with 21 woody species (Li et al., 2016) and a meta-analysis of available experimental data (Feng et al.,  
127 2018), the ~~dose-response relationship (DRR) shows~~ DRR showed convergent O<sub>3</sub> sensitivities for conifer  
128 and broadleaf trees if the area-based stomatal uptake was converted to the mass-based flux with LMA.  
129 ~~Meanwhile~~ This is likely related to the diluting effect of thicker leaves, which normally have stronger  
130 defenses against O<sub>3</sub> in their cross-section. Nowadays, a large number of trait observations were  
131 synthesized by global networks ~~in recent decades~~ (Gallagher et al., 2020). The TRY initiative (Kattge et  
132 al., 2011) ~~is was~~ one of the most influential datasets with 2.3 billion trait data by the year 2021. Based on  
133 the TRY dataset, global LMA was estimated with upscaling techniques such as Bayesian modeling (Butler  
134 et al., 2017) (thereafter B2017) or the random forest model (Moreno-Martinez et al., 2018) (thereafter  
135 M2018). These advances in the retrieval of LMA provide the possibility to depict more accurate O<sub>3</sub>  
136 vegetation damage at the global scale.

137

138 Here, we present a major advance in large-scale assessments of O<sub>3</sub> plant damage using a trait-based  
139 approach. We implement LMA into a stomatal flux-based O<sub>3</sub> damage framework aiming at a unified  
140 representation of plant O<sub>3</sub> sensitivities over the global grids. We couple this new approach to the Yale  
141 Interactive terrestrial Biosphere (YIBs) model (Yue and Unger, 2015) and evaluate the derived O<sub>3</sub>  
142 sensitivities against observations. We further assess contemporary O<sub>3</sub> impacts on global ~~gross primary~~  
143 ~~productivity (GPP)~~ in combination with the recently developed LMA datasets (Butler et al., 2017;  
144 ~~Gallagher et al., 2020~~; Moreno-Martinez et al., 2018; [Gallagher et al., 2020](#)) (Fig. ~~S1a1a~~) and the multi-  
145 model ensemble mean surface O<sub>3</sub> concentrations (Fig. ~~S1b1b~~). The updated risk map for O<sub>3</sub> vegetation  
146 damage is used to identify the regions and species with the largest sensitivity to O<sub>3</sub> threats.

147

## 148 2. Scheme development and calibration

### 149 2.1 The trait-based O<sub>3</sub> vegetation damage scheme

150 We develop the new scheme based on the ~~S2007~~[Sitch et al. \(2007\)](#) (hereafter ~~S2007~~) framework for  
151 transient O<sub>3</sub> damage calculation. In the original ~~S2007~~ scheme, the undamaged fraction  $F$  for net  
152 photosynthetic rate is dependent on the excessive area-based stomatal O<sub>3</sub> flux, which is calculated as the  
153 difference between  $f_{O_3}$  and PFT-specific area-based threshold  $y$ , and modulated by the sensitivity  
154 parameter  $a_{PFT}$ :

$$155 F = 1 - a_{PFT} \times \max\{f_{O_3} - y, 0\} \quad (1)$$

156 where  $a_{PFT}$  is calibrated and varies among PFTs with a typical range from “low” to “high” values  
157 indicating uncertainties of plant species within the same PFT ~~in Sitch et al. (2007)~~. The stomatal O<sub>3</sub> flux  
158  $f_{O_3}$  ( $\text{nmol m}^{-2} \text{s}^{-1}$ ) is calculated as:

$$159 f_{O_3} = \frac{[O_3]}{r + \left[ \frac{k_{O_3}}{g_p \times F} \right]} \quad (2)$$

160 where  $[O_3]$  is the O<sub>3</sub> concentration at the reference level ( $\text{nmol m}^{-3}$ ),  $r$  is the aerodynamic and boundary  
161 layer resistance between leaf surface and reference level ( $\text{s m}^{-1}$ ).  $k_{O_3}$  setting to 1.67 represents the ratio of  
162 leaf resistance for O<sub>3</sub> to that for water vapor.  $g_p$  represents potential stomata conductance for H<sub>2</sub>O ( $\text{m s}^{-1}$ ).  
163 <sup>1</sup>).

164

165 Studies suggested that LMA could be used to unify the area-based plant sensitivities to O<sub>3</sub> (Li et al., 2016;  
166 Feng et al., 2018; Li et al., 2016), resulting in a constant mass-based parameter  $a$  independent of plant  
167 species and PFTs:

$$168 \quad a = a_{PFT} \times LMA \quad (3)$$

169 Here, we convert the area-based O<sub>3</sub> stomatal flux expression in Equation (1) to a mass-based flux as  
170 follows:

$$171 \quad F = 1 - a \times \max \left\{ \frac{f_{O_3}}{LMA} - x, 0 \right\} \quad (4)$$

172 where the new sensitivity parameter  $a$  is a cross-species constant (nmol<sup>-1</sup> s g);  $LMA$  is leaf mass per area  
173 (g m<sup>-2</sup>); the flux threshold is replaced by a mass-based value of  $x$  (nmol g<sup>-1</sup> s<sup>-1</sup>) (Feng et al., 2018).

174 ~~This Equations (2) and (4) can form a quadratic equation is applied. The  $F$  can be derived at the each~~  
175 ~~timestep of photosynthesis calculation in the YIBs model (i.e. hourly) and applied to net photosynthetic~~  
176 ~~rate and stomatal conductance to calculate the O<sub>3</sub>-induced damages.~~ The updated LMA-based framework  
177 (YIBs-LMA) reduces the number of O<sub>3</sub> sensitivity parameters from three for each PFT (Sitch et al., 2007)  
178 in S2007 to a single parameter  $a$  for all PFTs. For YIBs-LMA framework, the default value of the  $x$   
179 threshold in Equation (4) is set to 0.019 nmol g<sup>-1</sup> s<sup>-1</sup> as recommended by Feng et al. (2018).

180

## 181 2.2 Dose-response relationship (DRR)

182 We compare the simulated and observed sensitivities to O<sub>3</sub> so as to calibrate the LMA-based scheme. In  
183 field experiments, DRR is used to quantify species-specific damage by O<sub>3</sub> with a generic format as follows:

$$184 \quad R = 100 + S_o \times \phi_{O_3} \quad (5)$$

185 where  $R$  (%) is the relative percentage of a ~~bio-biotic~~ indicator (such as biomass or yield) after and before  
186 O<sub>3</sub> damage;  $\phi_{O_3}$  is an area-based O<sub>3</sub> metric (e.g., POD<sub>y</sub> measured in sunlit leaves at the top of canopy);  
187  $S_o$  (usually negative) is the observed sensitivity derived as the slope of linear relationship between  $R$  and  
188  $\phi_{O_3}$ . We collected  $S_o$  from DRRs with conventional criteria (typically POD<sub>y=1</sub> for natural PFTs and  
189 POD<sub>y=6</sub> for crops as dose metrics (CLRTAP, 2017); ~~the bio-~~(Clrtap, 2017); ~~the biotic~~ indicators include  
190 the relative biomass for natural PFTs and relative yield for crops) among plant species from International  
191 Cooperative Programme on Effects of Air Pollution on Natural Vegetation and Crops (CLRTAP)

192 ~~(CLRTAP, 2017)~~(Clrtap, 2017) and multiple literature sources (Table S1). Such observations are used to  
193 calibrate the LMA-based scheme.

194

195 As a comparison with observations, we calculate annual relative GPP percentage ( $R_{GPP}$ , %) and  $POD_y$  of  
196 sunlit leaves in first canopy layer ( $\text{mmol m}^{-2} \text{ year}^{-1}$ , based on per leaf area) from the vegetation model to  
197 derive the slopes ( $S_S$ ) of simulated DRRs. Here,  $POD_y$  is a diagnostic variable calculated as:

$$198 \quad POD_y = \int (f_{O_3} - y) \frac{f_{O_3} - y}{\max\{f_{O_3} - y, 0\}} = \int \max\{f_{O_3} - y, 0\} \\ 199 \quad (6)$$

200 where  $f_{O_3}$  represents the stomatal  $O_3$  flux under instant  $O_3$  stimulus at each timestep, which can be  
201 calculated following Equation (2) on the leaf level;  $y$  is the prescribed critical level ( $1 \text{ nmol m}^{-2} \text{ s}^{-1}$  for  
202 natural or  $6 \text{ nmol m}^{-2} \text{ s}^{-1}$  for crop species ~~(CLRTAP, 2017)~~). ~~Excessive  $O_3$  flux above  $y$  is accumulated~~  
203 ~~for~~(Clrtap, 2017)). Excessive  $O_3$  flux above  $y$  is accumulated for the sunlit leaves of the top canopy layer  
204 and over the growing season to derive the  $POD_y$ . Simulated  $S_S$  is calculated as the slope of the regression  
205 between simulated  $R_{GPP}$  (%) and  $POD_y$  at the PFT level. Only the dominant PFT in each grid is considered  
206 for the estimate of  $S_S$  at both PFT-level or gridded analyses.

207

208 Similarly, mass-based  $POD_x$  is derived from  $O_3$ -impacted  $f_{O_3}$  ( $\text{nmol m}^{-2} \text{ s}^{-1}$ ) in Equation (2), together with  
209 gridded LMA ( $\text{g m}^{-2}$ ) and mass-based threshold  $x$  ( $\text{nmol g}^{-1} \text{ s}^{-1}$ ) as:

$$210 \quad POD_x = \int \left( \frac{f_{O_3}}{LMA} - x \right) \frac{f_{O_3}}{LMA} - x \quad (7)$$

211

### 212 **2.3 Simulations and calibrations**

213 We perform two groups of supporting experiments (Table 1). The first group explores modeling  
214 uncertainties associated with the mass-based framework: (1) YIBs-LMA\_B2017 replaces the default  
215 LMA map of M2018 (Moreno-Martinez et al., 2018) with B2017 (Butler et al., 2017). (2) YIBs-  
216 LMA\_PFT applies PFT-specific LMA values (Table S2) for each PFT without considering global LMA  
217 geo-gradient. (3) YIBs-LMA\_T replaces the default threshold of  $x=0.019 \text{ nmol g}^{-1} \text{ s}^{-1}$  with  $x=0.006 \text{ nmol}$   
218  $\text{g}^{-1} \text{ s}^{-1}$ , which is an alternative parameter suggested by observations (Feng et al., 2018). The second group  
219 of supporting experiments explores the differences between mass-based and S2007 area-based

220 frameworks. Typically, S2007 has a “low to high”  $a_{PFT}$  range for each PFT. Here, a mean sensitivity  
221 parameterization of S2007 (YIBs-S2007\_adj) is re-calibrated according to  $S_O$  in Table S1.

222

223 For all supporting experiments, the parameter  $a$  for YIBs-LMA or the eight mean  $a_{PFT}$  for YIBs-  
224 S2007\_adj are derived with the optimal 1:1 fitting between  $S_S$  and  $S_O$  to minimize the possible biases  
225 (Tables ~~S3-S7~~, 2 and S3-S6). The basic method for calibration is feeding the model with series values of  
226  $a$  or  $a_{PFT}$  until the predicted  $O_3$  damage matches observations with the lowest normalized mean biases  
227 (NMB). For all LMA-based experiments,  $S_S$  from varied PFTs were grouped for the calibration of  $a$ , while  
228 for  $a_{PFT}$  in YIBs-S2007\_adj, each  $a_{PFT}$  is determined individually by matching simulated  $S_S$  with  $S_O$ . Since  
229  $S_O$  are available only for six out of the eight YIBs PFTs, including EBF, NF, DBF, C<sub>3</sub> grass, C<sub>4</sub> grass, and  
230 crop (Table S1),  $S_O$  of these PFTs are used for calibration. All runs are summarized in Table 1.

231

## 232 **2.4 YIBs model and forcing data**

233 In this study, all  $O_3$  vegetation damage schemes are implemented in the YIBs model (Yue and Unger,  
234 2015). ~~The YIBs, which~~ is a process-based dynamic global vegetation model incorporated with well-  
235 established carbon, energy, and water interactive schemes. The model applies the same PFT  
236 classifications as the Community Land Model (Bonan et al., 2003) (Fig. ~~S2S1~~). Eight PFTs are employed  
237 including evergreen broadleaf forest (EBF), needleleaf forest (NF), deciduous broadleaf forest (DBF),  
238 cold shrub (C\_SHR), arid shrubland (A\_SHR), C<sub>3</sub> grassland (C3\_GRA), C<sub>4</sub> grassland (C4\_GRA), and  
239 cropland (CRO) (Fig. ~~S2S1~~). For each PFT, phenology is well-evaluated (Yue and Unger, 2015) to  
240 generate a reliable growing season, which is crucial for the simulation of stomatal  $O_3$  uptake (Anav et al.,  
241 2018). Photosynthesis and stomatal processes are calculated using Farquhar et al. and Ball-Berry  
242 algorithms (~~Ball et al., 1987~~; Farquhar et al., 1980; Ball et al., 1987), respectively. Leaf area index (LAI)  
243 and tree height are predicted dynamically based on vegetation carbon allocation. The YIBs model has  
244 joined the multi-model ensemble project TRENDY and showed reasonable performance in the  
245 simulations of global biomass, GPP, LAI, net ecosystem exchange, and soil carbon relative to  
246 observations (Friedlingstein et al., 2020). Key plant biogeochemical parameters of the YIBs model are  
247 adjusted for this research (Table ~~S8S7~~).

248

249 The hourly modern-era retrospective analysis for research and applications version 2 (MERRA2) climate  
250 reanalyses (Gelaro et al., 2017) are used to drive the YIBs model. The gridded LMA required for the main  
251 mass-based simulation is derived from Moreno-Martinez et al. (2018) (M2018), which shows the highest  
252 value of  $>150 \text{ g m}^{-2}$  for needleleaf forest at high latitudes while low values of  $\sim 40 \text{ g m}^{-2}$  for grassland and  
253 cropland (Fig. [S1a1a](#) and Fig. [S2S1](#)). Grids with missing LMA data are filled with the mean of the  
254 corresponding PFT. Contemporary  $\text{O}_3$  concentration fields in the year of 2010 from the multi-model mean  
255 in Task Force on Hemispheric Transport of Air Pollutants (TF-HTAP) experiments (Turnock et al., 2018)  
256 (Fig. [S1b1b](#)) are used as forcing data. The original monthly  $\text{O}_3$  data are downscaled to hourly using the  
257 diurnal cycle predicted by the chemistry-climate-carbon fully coupled model ModelE2-YIBs (Yue and  
258 Unger, 2015). Generally, areas of severe  $\text{O}_3$  pollution are found in the mid-latitudes of the Northern  
259 Hemisphere with highest annual average  $\text{O}_3$  concentration of over 40 ppbv in East Asia. All data are  
260 interpolated to the spatial resolution of  $1^\circ \times 1^\circ$ .

261

### 262 3. Results

#### 263 3.1 Comparison of simulated sensitivities with observations

264 Simulated relative GPP percentage ( $R_{\text{GPP}}$ ) at global grids were sorted by dominant PFTs (Fig. [S2S1](#)) and  
265 plotted against area-based accumulated phytotoxic  $\text{O}_3$  dose above a threshold  $y \text{ nmol m}^{-2} \text{ s}^{-1}$  ( $\text{POD}_{y=1}$ ) at  
266 the corresponding grids (Fig. [12](#)). The DRR shows varied slopes among different PFTs, resulting in a  
267 coefficient of determination ( $R^2$ ) around 0.54 for all PFTs (Figs [1a-1e2a-2c](#)). We further calculated the  
268 mass-based accumulated phytotoxic  $\text{O}_3$  dose above a threshold of  $0.019 \text{ nmol g}^{-1}$  ( $\text{POD}_{x=0.019}$ ) and  
269 compared it with  $R_{\text{GPP}}$ . The updated DRR showed convergent slopes and reached a high  $R^2$  of 0.77 across  
270 all PFTs (Figs [1d-1f2d-2f](#)), suggesting that the mass-based scheme could better unify  $\text{O}_3$  sensitivities  
271 among different PFTs.

272

273 We then calibrated the single, best-fit  $a$  value for the YIBs-LMA framework by minimizing the absolute  
274 difference between simulated ( $S_S$ ) and observed ( $S_O$ ) slopes of  $\text{O}_3$  DRR for all PFTs. With different  $a$   
275 parameters, the YIBs-LMA framework yielded considerably high  $R^2$  of  $\sim 1.0$  but varied biases between

276 simulated and observed O<sub>3</sub> impacts across PFTs (Fig. 23). Both the 1:1 fitting and the lowest bias between  
277  $S_S$  and  $S_O$  were achieved with an optimal  $a = 3.5 \text{ nmol}^{-1} \text{ s g}$  (Fig. 2e-3c). Notably, such calibration of  $a$  is  
278 robust under different O<sub>3</sub> field (see Fig. S2). Consistent with observations, YIBs-LMA with this optimal  
279  $a$  parameter simulated low  $S_S$  of -0.18% and -0.36% per  $\text{mmol m}^{-2} \text{ year}^{-1}$  of  $\text{POD}_{y=1}$  for evergreen  
280 broadleaf forest and needleleaf forest, respectively (Figs 3a4a, b), median  $S_S$  from -0.53% per  $\text{mmol m}^{-2}$   
281  $\text{year}^{-1}$  for arid shrubland (Fig. 3e4e), and high  $S_S$  from -0.64% to -1.04% per  $\text{mmol m}^{-2} \text{ year}^{-1}$  for deciduous  
282 broadleaf forest, C<sub>3</sub>/C<sub>4</sub> grassland, cropland and cold shrubland (-3.28% for crops with  $\text{POD}_{y=6}$ , Figs 3e4c-  
283 d, 3f4f-h).

284

### 285 3.2 Global map of O<sub>3</sub> vegetation damage

286 We estimated contemporary GPP reductions induced by O<sub>3</sub> with the global concentrations of surface O<sub>3</sub>  
287 (Fig. S1b1b) in the year of 2010. The YIBs-LMA framework using an increase of  $a$  parameter yielded an  
288 almost linearly linear enhancement of global GPP reduction (Fig. S3) with consistent spatial distributions  
289 (Fig. S4). The simulation with the optimal  $a = 3.5 \text{ nmol}^{-1} \text{ s g}$  predicted a global GPP reduction of 4.8%  
290 (Fig. 4a5a), which was similar to the value estimated with the area-based S2007 scheme (YIBs-S2007\_adj,  
291 Table 1). Large reductions of >10% were predicted over the eastern U.S., western Europe, eastern China,  
292 and India (Fig. 4a5a). Hotspots were mainly located in cropland and agricultural areas mixed with  
293 deciduous broadleaf forest or grassland, accompanied withby moderate to high levels of surface O<sub>3</sub>. Few  
294 discrepancies between the damage maps of YIBs-LMA and YIBs-S007\_adj were found (Fig. 4b5b and  
295 Fig. S5), even though the number of parameters was greatly reduced in the YIBs-LMA scheme.

296

297 For YIBs-LMA, PFTs with low LMA such as cropland, grassland, and deciduous broadleaf forest account  
298 for 73.3 Pg C yr<sup>-1</sup> (50.0%) of the global GPP (Table S9S8). However, these PFTs contributed to a total  
299 GPP reduction of 5.4 Pg C yr<sup>-1</sup> (75.5% of total GPP loss) by O<sub>3</sub> damage. In contrast, evergreen broadleaf  
300 and needleleaf forests with high LMA accounted for 48.8 Pg C yr<sup>-1</sup> (33.0%) of total GPP but yielded only  
301 a reduction of 0.75 Pg C yr<sup>-1</sup> (10.5% of total GPP loss). Differences in GPP percentage losses were in part  
302 associated with the global pattern of O<sub>3</sub> concentrations, which were usually higher over mid-latitudes with  
303 populated cities and dense crop plantations (Fig. S1b1b). However, the differences in LMA and simulated



304 O<sub>3</sub> sensitivities of these PFTs ~~were the main cause of~~ also made important contributions to such  
305 discrepancies in GPP damage at the large scaled damages.

306

### 307 **3.3 Uncertainties of the LMA-based scheme**

308 We quantified the uncertainties of the LMA-based ~~scheme~~ scheme by comparing simulated GPP damages  
309 among different experiments (Table 1). The experiment with the alternative LMA map of B2017 (Fig.  
310 ~~S5S6~~) showed similar spatial patterns but a slightly enhanced GPP reduction of 5.3% (Fig. ~~5a~~) but similar  
311 spatial patterns (6a) compared ~~with YIBs-LMA to the simulations~~ using LMA map of M2018 (Fig. ~~4a~~)  
312 ~~However, 5a~~). The B2017 map has a much less source of LMA data than M2018 (~40%), leading to some  
313 unexpected areas with high O<sub>3</sub> threats such as over the tundra in the Arctic ~~region~~ (Fig. ~~S6~~) ~~The S7~~).  
314 Another experiment ~~with using~~ PFT-specific LMA estimated a global GPP reduction of 4.6% (Fig. ~~5b6b~~)  
315 with a consistent spatial pattern as the prediction within YIBs-LMA, suggesting ~~the reasonable~~  
316 ~~application of that the~~ PFT-level LMA at can be used in case of the lack of ~~global regional~~ LMA data. The  
317 third experiment with an alternative threshold flux (Feng et al., 2018) of 0.006 nmol g<sup>-1</sup> s<sup>-1</sup> estimated a  
318 higher high GPP reduction of 6.5% ~~by global O<sub>3</sub>~~ (Fig. ~~5e~~) ~~with 6c~~) due to the overestimations of O<sub>3</sub>  
319 sensitivities for some tree PFTs (Fig. ~~67~~). The fourth run, YIBs-S2007 adj ~~run using recalibrated PFT-~~  
320 ~~level sensitivities predicts, predicted~~ a similar global GPP damage of 4.8% as the YIBs-LMA run with a  
321 high spatial correlation coefficient of 0.98 (Fig. ~~5d~~) ~~6d~~). Such good consistency is mainly due to the  
322 application of recalibrated PFT-level sensitivities in YIBs-S2007 adj. Finally, we tested a new calibration  
323 excluding CRO, the PFT that contributed the most to the calibration biases (shown as orange dashed lines  
324 in Fig. S8). The results gave an optimal  $\alpha$  of 3.2, with global damage of 4.5%. All sensitivity experiments  
325 ~~achieve~~ achieved consistent results as the YIBs-LMA simulation with ~~an uncertainty ranged damages~~  
326 ranging from ~~-0.24.5%~~ to 1.76.5% and spatial correlation coefficients larger than 0.94.

327

## 328 **4. Discussion**

### 329 **4.1 Mechanisms behind the LMA-based approach**

330 In recent decades, the plant science community examined how traits could be used to differentiate and  
331 predict the functions of plant species (Reich et al., ~~1999~~ 1997; Reich et al., ~~1997~~ 1999). LMA, related to



332 leaf density and thickness, is a key trait reflecting many aspects of leaf function (Reich et al., 1998). In  
333 the field of O<sub>3</sub> phytotoxicology, experiments have revealed plants with high LMA usually have thick  
334 leaves with physical and chemical defenses (Poorter et al., 2009), which can strengthen their resistance  
335 to O<sub>3</sub> ([Li et al., 2016](#); [Feng et al., 2018](#); [Li et al., 2016](#)). On the contrary, plants with low LMA normally  
336 have thin leaves which are likely to be less O<sub>3</sub>-tolerant ([Li et al., 2016](#); [Feng et al., 2018](#); [Li et al., 2016](#)).  
337 Moreover, it seems plausible that the oxidative stress caused by a given amount of stomatal O<sub>3</sub> flux per  
338 unit leaf area would be distributed over a larger leaf mass, and hence diluted, in a leaf with high LMA.  
339 Such [LMA-O<sub>3</sub>](#) sensitivity relationship can be well reproduced by our LMA-based model (Figs [7a8a](#)  
340 and [7b8b](#)). Below we explore the linkage between O<sub>3</sub> plant sensitivities and the mutual adaptation of  
341 growth strategies and leaf morphology with plant leaf trade-off theory (Reich et al., 1999; Shipley et al.,  
342 2006).

343

344 In the natural world, plants often adapt to maximize carbon uptake under prevailing conditions (Reich et  
345 al., 1998; Shipley et al., 2006). To make full use of resources in the growing season, leaves under varied  
346 living conditions choose either fast photosynthetic rates (fast-growing deciduous types) or long  
347 photosynthesis duration (slow-growing evergreen types) with compatible leaf structures ([Reich, 2014](#);  
348 [Diaz et al., 2016](#); [Reich, 2014](#)). The former species expand leaf area (low LMA) to maximize light  
349 interception while the latter species produce thick and mechanically strong leaves (high LMA) with ample  
350 resistant substances for durable utilization (Poorter et al., 2009) in resource-limited and/or environment-  
351 stressed habitats (Wright et al., 2002). As a side effect of such leaf trade-offs, deciduous plants with their  
352 high rates of photosynthesis, associated large stomatal conductance (Davison and Barnes, 1998; Henry et  
353 al., 2019), and less total defense capacity through the leaf profile (Poorter et al., 2009), are highly O<sub>3</sub>  
354 sensitive (Mode1 in Fig. [89](#)). In contrast, the moderate photosynthesis, relatively low maximum stomatal  
355 conductance (Davison and Barnes, 1998; Henry et al., 2019), and reinforced dense leaves (Poorter et al.,  
356 2009) lead to low sensitivity for evergreen plants (Mode2 in Fig. [89](#)). Therefore, in our  
357 [modellingmodeling](#) practice, the mass-based O<sub>3</sub> gas exchange algorithm can be regarded as taking into  
358 account several interrelated factors such as growth-driven gas exchange requirements, gas path length,  
359 and biochemical reserves, in a unified, simplified and effective manner via LMA.

360

## 361 **4.2 Implication of potential risks for fast-growing plants**

362 Our new approach reflected the general experimental findings that deciduous plants are much more  
363 vulnerable to O<sub>3</sub> than evergreen species ([Li et al., 2017](#); Feng et al., 2018; ~~Li et al., 2017~~), and in turn  
364 within a PFT, early-successional/pioneers with low LMA are likely more vulnerable than late-  
365 successional/canopy trees with high LMA (Fyllas et al., 2012). This law has been neglected in previous  
366 modeling studies due to the dependence on the limited observed data used for PFT-specific tuning. Our  
367 LMA-based approach bridges this gap through grid-based parameterization, and in addition, our data-  
368 model integration specifically emphasizes the broad high risks for fast-growing plants, especially for  
369 crops. Among PFTs, crops may endure the largest O<sub>3</sub> threats (Davison and Barnes, 1998; Feng et al.,  
370 2021; Mukherjee et al., 2021) because they are artificially bred with high photosynthetic capacities  
371 (Richards, 2000), stomatal conductance, generally low LMA (Bertin and Gary, 1998; [Li et al., 2018](#);  
372 Wang and Shangguan, 2010; Wu et al., [2018](#); [Li et al., 2018](#)) (roughly 30-60 g m<sup>-2</sup>), and cultivated in  
373 populated regions with high ambient O<sub>3</sub> concentrations. Modern technology aims to promote crop yield  
374 (Herdt, 2005), but this can potentially elevate crop sensitivities to O<sub>3</sub> (Biswas et al., ~~2013~~[2008](#); Biswas et  
375 al., ~~2008~~[2013](#)). This study estimated the highest annual mean GPP damage for crop, 12.6%, which is at  
376 the high end of the 4.4-12.4% of the O<sub>3</sub>-induced yield loss estimated for global modeling of soybean,  
377 wheat, rice, and maize (Mills et al., ~~2018b~~[2018a](#)). Furthermore, human-induced land use activities may  
378 also increase O<sub>3</sub> damage risks. The global demand for food and commodities leads to the conversion of  
379 natural forests to irrigated croplands, grazing pastures, and economical-tree plantations (Curtis et al., 2018;  
380 Zalles et al., 2021). Meanwhile, the urgent actions to combat climate change promote large-scale  
381 afforestation and reforestation (Cook-Patton et al., 2020). These land use changes with fast-growing plant  
382 species may increase the risks of terrestrial ecosystems to surface O<sub>3</sub>.

383

## 384 **4.3 Advances in the global O<sub>3</sub> damage assessment**

385 For the first time, we implemented plant trait LMA into a process-based O<sub>3</sub> impact modeling scheme and  
386 obtained reasonable interspecific and inter-PFT O<sub>3</sub> responses supported by observations. ~~This LMA-~~  
387 ~~based approach indicates an important advance in global O<sub>3</sub> damage assessments. The similarity between~~

388 YIBs-S2007 and YIBs-LMA shown in Fig. 5 revealed an advance in the modeling strategy. Simulated O<sub>3</sub>  
389 damage in YIBs-S2007 is based on the PFT-level calibrations that tuned sensitivity parameters of each  
390 PFT with observed DRRs. Such refinement is a data-driven approach without clear physical reasons.  
391 Instead, the YIBs-LMA framework converts the area-based responses to mass-based ones and achieves  
392 better unification in O<sub>3</sub> sensitivities among different PFTs. In this algorithm, the O<sub>3</sub> damage efficiency is  
393 inversely related to plant LMA, which influences both the O<sub>3</sub> uptake potential and the detoxification  
394 capability of the vegetation. The similarity in the global assessment of O<sub>3</sub> vegetation damage between  
395 YIBs-S2007 and YIBs-LMA further demonstrated the physical validity of LMA-based scheme in the  
396 Earth system modeling, because the independent LMA map was applied in the latter approach.

397

398 In addition to the advance in physical mechanisms, the LMA-based approach improves global O<sub>3</sub> damage  
399 assessments in the following aspects. First, it significantly reduces the number of required key parameters.  
400 To account for interspecific sensitivities, many schemes have to define PFT-level parameters to cap the  
401 ranges of plant responses (Sitch et al., 2007; Felzer et al., 2009; Lombardozzi et al., 2015; ~~Sitch et al.,~~  
402 ~~2007~~). As a result, those schemes rely on dozens of parameters which ~~increase~~increases the uncertainties  
403 of modeling and the difficulties for model calibration. The LMA-based approach requires the calibration  
404 of one single parameter  $\alpha$ , largely facilitating its application across different vegetation models. Second,  
405 the new approach accounts for the continuous spectrum of O<sub>3</sub> sensitivities. Previous studies usually  
406 categorized species into groups of low or high O<sub>3</sub> sensitivity, depending on very limited data from O<sub>3</sub>  
407 exposure experiments. As a result, gridcells for a specific PFT share the same sensitivities regardless of  
408 their geographic locations and ecosystem characteristics. In reality, there are hundreds and thousands of  
409 plant species in each PFT and they usually have large ~~variation~~variations in biophysical parameters  
410 including LMA and O<sub>3</sub> sensitivities. The LMA-based approach takes advantage of the newly revealed  
411 unifying concept in O<sub>3</sub> sensitivity (Li et al., 2016; Feng et al., 2018; Li et al., ~~2016~~; ~~Li et al., 2022~~) and  
412 the recent development in a trait-based LMA global map (Fig. ~~S1a1a~~). Such configurations present a  
413 spectrum of gridded O<sub>3</sub> sensitivities (Fig. ~~7a8a~~) following the variations of LMA distribution.

414

415 **4.4 Outlook for future modeling**

416 In nature, all aspects of plant physiochemical processes, such as growth, development, reproduction, and  
417 bringdefense, are influenced by abiotic factors like water availability, temperature, CO<sub>2</sub> concentration,  
418 and light resources (Kochhar and Gujral, 2020). In our modeling, the possibility of capturing cumulative  
419 O<sub>3</sub> fluxes are based on dynamic plant simulations with well-established DGVM to calculate the effects of  
420 these abiotic factors. LMA is considered as a factor representing the vulnerability of each species, by  
421 which divergent responses to the same O<sub>3</sub> stomatal dose can be further differentiated. In fact, many other  
422 key variables in DGVMs, for example, leaf photosynthetic traits (V<sub>cmax</sub> and J<sub>max</sub>), nutrient traits (leaf  
423 nitrogen and phosphorus), morphological traits (leaf thickness and size), and phenology-related traits (leaf  
424 life span) are all more or less interlinked with LMA (Walker et al., 2014). There are some generic  
425 regression relationships between them, which have not yet been fully validated by experimental studies.  
426 As a result, considerable improvements can be made in the direction of trait-flexible modeling within the  
427 existing DGVM frameworks. Our study demonstrates the validity of LMA-based approach for the O<sub>3</sub>  
428 plant damage modeling.

429

430 Although we used the most advanced LMA integrated from available observations, this dataset was  
431 developed based on static global grids and revealed the mean state for each pixel. In reality, LMA can  
432 vary with biotic/abiotic factors like leaf position in the canopy (Keenan and Niinemets, 2017), phenology,  
433 plant health, living environment (Fritz et al., 2018), and climate (Wright et al., 2005; Cui et al., 2020).  
434 Even long-term exposure to O<sub>3</sub> can alter leaf morphological characteristics and LMA (Li et al., 2017). In  
435 future studies, simulations from local to global scales could implement the spatiotemporal variation in  
436 vegetation O<sub>3</sub> sensitivity through time-sensitive LMA products in the future. variations in LMA taking  
437 into account the demographic information and environmental forcings. We expect a breakthrough in the  
438 calculation of reliable LMA to achieve fully dynamic predictions of O<sub>3</sub> plant damage in Earth System  
439 Modeling, thus facilitating the research of plant response and adaption in changing environments.

440

441

442 **Code availability**

443 The codes of YIBs model with LMA-based O<sub>3</sub> damaging scheme are shared at  
444 <https://zenodo.org/record/6348731>.

445

#### 446 **Data availability**

447 Results of all simulations (listed in Table 1) are available upon request. Data for Figures in the main  
448 article are shared at <https://zenodo.org/record/6348731>. The global maps of specific leaf area (SLA) to  
449 derive LMA for M2018 and B2017 are from <https://www.try-db.org/TryWeb/Data.php#59> and  
450 [https://github.com/abhirupdatta/global\\_maps\\_of\\_plant\\_traits](https://github.com/abhirupdatta/global_maps_of_plant_traits), respectively. Monthly O<sub>3</sub> data is from  
451 <https://doi.org/10.5194/acp-18-8953-2018>. Calibration data are summarized in Table S1.

452

#### 453 **Author Contributions**

454 X.Y., S.S. and N.U. designed the research, Y.M.M. performed modeling, data analyses, virtualization and  
455 wrote the draft. J.U, L.M., Z.Z.F, and A.W.C advised on concepts and methods. C.G. helped write draft.  
456 H.Y.Y., M.C.D.R helped with coding. H.Z., C.G.T., Y.C., Y.D.L., and Y.S.X. helped with data collection.  
457 All authors commented and revised the manuscript.

458

#### 459 **Competing interests**

460 The authors declare no conflict of interests.

461

#### 462 **Financial support**

463 Xu Yue acknowledges funding ~~support from~~ supports from the National Natural Science Foundation of  
464 China (grant no. 42275128) and Jiangsu Science Fund for Distinguished Young Scholars (grant no.  
465 BK20200040). Yimian Ma acknowledges financial support from China Scholarship Council (CSC no.  
466 201804910712). Johan Uddling acknowledges the strategic research area Biodiversity and Ecosystems in  
467 a Changing Climate, BECC. SS, NU, LM, AC were supported by NERC funding (NE/R001812/1).

468

#### 469 **References**

470 [Ainsworth, E., Agathokleous, E., Feng, Z., Oksanen, E., Sicard, P., Wang, Q., Saitanis, C. J., Araminiene, V., Blande, J. D., Hayes, F.,](#)  
471 [Calatayud, V., Domingos, M., Veresoglou, S. D., Penuelas, J., Wardle, D. A., De Marco, A., Li, Z., Harmens, H., Yuan, X., Vitale, M., and](#)

472 [Paoletti, E.: Ozone affects plant, insect, and soil microbial communities: A threat to terrestrial ecosystems and biodiversity, \*Sci Adv\*, 6,](#)  
473 [10.1126/sciadv.abc1176, 2020.](#)

474 [Ainsworth, E. A., Lemonnier, P., and Wedow, J. M.: The influence of rising tropospheric carbon dioxide and ozone on plant productivity,](#)  
475 [Plant Biology, 22, 5-11, 10.1111/plb.12973, 2020.](#)

476 [Ainsworth, E. A., Yendrek, C. R., Sitch, S., Collins, W. J., and Emberson, L. D.: The Effects of Tropospheric Ozone on Net Primary](#)  
477 [Productivity and Implications for Climate Change, \*Annu Rev Plant Biol\*, 63, 637-661, 2012-10.1146/Annurev-Arplant-042110-103829,](#)  
478 [2012.](#)

479 [Anav, A., Liu, Q., De Marco, A., Proietti, C., Savi, F., Paoletti, E., and Piao, S.: The role of plant phenology in stomatal ozone flux modeling,](#)  
480 [Global Change Biol, 24, 235-248, 10.1111/gcb.13823, 2018.](#)

481 [Ball, J. T., Woodrow, I. E., and Berry, J. A.: A model predicting stomatal conductance and its contribution to the control of photosynthesis](#)  
482 [under different environmental conditions, \*Progress in Photosynthesis Research: Viith International Congress on Photosynthesis\*, doi:](#)  
483 [10.1007/978-94-017-0519-6\\_48, 1987.](#)

484 [Bertin, N. and Gary, C.: Short and long term fluctuations of the leaf mass per area of tomato plants - Implications for growth models, \*Ann\*](#)  
485 [Bot-London, 82, 71-81, DOI 10.1006/anbo.1998.0647, 1998.](#)

486 [Biswas, D. K., Xu, H., Li, Y. G., Ma, B. L., and Jiang, G. M.: Modification of photosynthesis and growth responses to elevated CO<sub>2</sub> by](#)  
487 [ozone in two cultivars of winter wheat with different years of release, \*J Exp Bot\*, 64, 1485-1496, 10.1093/jxb/ert005, 2013.](#)

488 [Biswas, D. K., Xu, H., Li, Y. G., Sun, J. Z., Wang, X. Z., Han, X. G., and Jiang, G. M.: Genotypic differences in leaf biochemical,](#)  
489 [physiological and growth responses to ozone in 20 winter wheat cultivars released over the past 60 years, \*Global Change Biol\*, 14, 46-59,](#)  
490 [10.1111/j.1365-2486.2007.01477.x, 2008.](#)

491 [Bonan, G. B., Levis, S., Sitch, S., Vertenstein, M., and Oleson, K. W.: A dynamic global vegetation model for use with climate models:](#)  
492 [concepts and description of simulated vegetation dynamics, \*Global Change Biol\*, 9, 1543-1566, 10.1046/J.1365-2486.2003.00681.X, 2003.](#)

493 [Buker, P., Feng, Z., Uddling, J., Briolat, A., Alonso, R., Braun, S., Elvira, S., Gerosa, G., Karlsson, P. E., Le Thiec, D., Marzuoli, R., Mills,](#)  
494 [G., Oksanen, E., Wieser, G., Wilkinson, M., and Emberson, L. D.: New flux based dose-response relationships for ozone for European forest](#)  
495 [tree species, \*Environ- Pollut\*, 206, 163-174, 10.1016/j.envpol.2015.06.033, 2015.](#)

496 [Butler, E. E., Datta, A., Flores-Moreno, H., Chen, M., Wythers, K. R., Fazayeli, F., Banerjee, A., Atkin, O. K., Kattge, J., Amiaud, B.,](#)  
497 [Blonder, B., Boenisch, G., Bond-Lamberty, B., Brown, K. A., Byun, C., Campetella, G., Cerabolini, B. E. L., Cornelissen, J. H. C., Craine,](#)  
498 [J. M., Craven, D., de Vries, F. T., Diaz, S., Domingues, T. F., Forey, E., Gonzalez-Melo, A., Gross, N., Han, W., Hattingh, W. N., Hickler,](#)  
499 [T., Jansen, S., Kramer, K., Kraft, N. J. B., Kurokawa, H., Laughlin, D. C., Meir, P., Minden, V., Niinemets, U., Onoda, Y., Penuelas, J.,](#)  
500 [Read, Q., Sack, L., Schamp, B., Soudzilovskaia, N. A., Spasojevic, M. J., Sosinski, E., Thornton, P. E., Valladares, F., van Bodegom, P. M.,](#)  
501 [Williams, M., Wirth, C., and Reich, P. B.: Mapping local and global variability in plant trait distributions, \*Proc Natl Acad Sci U S A\*, 114,](#)  
502 [E10937-E10946, 10.1073/pnas.1708984114, 2017.](#)

503 [CLRTAP: The UNECE Convention on Long-range Transboundary Air Pollution, Manual on Methodologies and Criteria for Modelling and](#)  
504 [Mapping Critical Loads and Levels and Air Pollution Effects, Risks and Trends: Chapter III Mapping Critical Levels for Vegetation, 2017.](#)  
505 [2017.](#)

506 [Cook-Patton, S. C., Leavitt, S. M., Gibbs, D., Harris, N. L., Lister, K., Anderson-Teixeira, K. J., Briggs, R. D., Chazdon, R. L., Crowther,](#)  
507 [T. W., Ellis, P. W., Griscom, H. P., Herrmann, V., Holl, K. D., Houghton, R. A., Larrosa, C., Lomax, G., Lucas, R., Madsen, P., Malhi, Y.,](#)  
508 [Paquette, A., Parker, J. D., Paul, K., Routh, D., Roxburgh, S., Saatchi, S., van den Hoogen, J., Walker, W. S., Wheeler, C. E., Wood, S. A.,](#)  
509 [Xu, L., and Griscom, B. W.: Mapping carbon accumulation potential from global natural forest regrowth, \*Nature\*, 585, 545-550,](#)  
510 [10.1038/s41586-020-2686-x, 2020.](#)

511 [Cui, E., Weng, E., Yan, E., and Xia, J.: Robust leaf trait relationships across species under global environmental changes, \*Nat Commun\*, 11,](#)  
512 [2999, 10.1038/s41467-020-16839-9, 2020.](#)

513 [Curtis, P. G., Slay, C. M., Harris, N. L., Tyukavina, A., and Hansen, M. C.: Classifying drivers of global forest loss, \*Science\*, 361, 1108-](#)  
514 [1111, 10.1126/science.aau3445, 2018.](#)

515 [Davison, A. W. and Barnes, J. D.: Effects of ozone on wild plants, \*New Phytol\*, 139, 135-151, 1998-https://doi.org/10.1046/j.1469-](#)  
516 [8137.1998.00177.x, 1998.](#)

517 [Diaz, S., Kattge, J., Cornelissen, J. H., Wright, I. J., Lavorel, S., Dray, S., Reu, B., Kleyer, M., Wirth, C., Prentice, I. C., Garnier, E., Bonisch,](#)  
518 [G., Westoby, M., Poorter, H., Reich, P. B., Moles, A. T., Dickie, J., Gillison, A. N., Zanne, A. E., Chave, J., Wright, S. J., Sheremet'ev, S.](#)  
519 [N., Jactel, H., Baraloto, C., Cerabolini, B., Pierce, S., Shipley, B., Kirkup, D., Casanoves, F., Joswig, J. S., Gunther, A., Falczuk, V., Ruger,](#)  
520 [N., Mahecha, M. D., and Gorne, L. D.: The global spectrum of plant form and function, \*Nature\*, 529, 167-171, 10.1038/nature16489, 2016.](#)

521 [Emberson, L. D., Pleijel, H., Ainsworth, E. A., van den Berg, M., Ren, W., Osborne, S., Mills, G., Pandey, D., Dentener, F., Buker, P., Ewert,](#)  
522 [F., Koeble, R., and Van Dingenen, R.: Ozone effects on crops and consideration in crop models, \*Eur J Agron\*, 100, 19-34,](#)  
523 [10.1016/j.eja.2018.06.002, 2018.](#)

524 [Farquhar, G. D., Caemmerer, S. V., and Berry, J. A.: A biochemical-model of photosynthetic CO<sub>2</sub> assimilation in leaves of C<sub>3</sub> Species,](#)  
525 [Planta, 149, 78-90, 10.1007/Bf00386231, 1980.](#)



526 [Felzer, B., Kicklighter, D., Melillo, J., Wang, C., Zhuang, Q., and Prinn, R.: Effects of ozone on net primary production and carbon](#)  
527 [sequestration in the conterminous United States using a biogeochemistry model, \*Tellus B\*, 56, 230-248, \[https://doi.org/10.1111/j.1600-\]\(https://doi.org/10.1111/j.1600-0889.2004.00097.x\)](#)  
528 [0889.2004.00097.x, 2004.](#)

529 Felzer, B. S., Cronin, T. W., Melillo, J. M., Kicklighter, D. W., and Schlosser, C. A.: Importance of carbon-nitrogen interactions and ozone  
530 on ecosystem hydrology during the 21st century, *J. Geophys. Res.*, 114, G01020, [10.1029/2008jg000826](https://doi.org/10.1029/2008jg000826), 2009.

531 [Feng, Z., Xu, Y., Kobayashi, K., Dai, L., Zhang, T., Agathokleous, E., Calatayud, V., Paoletti, E., Mukherjee, A., Agrawal, M., Park, R. J.,](#)  
532 [Oak, Y. J., and Yue, X.: Ozone pollution threatens the production of major staple crops in East Asia, \*Nature Food\*, 3, 47-56, \[10.1038/s43016-\]\(https://doi.org/10.1038/s43016-021-00422-6\)](#)  
533 [021-00422-6, 2022.](#)

534 Feng, Z., Agathokleous, E., Yue, X., Oksanen, E., Paoletti, E., Sase, H., Gandin, A., Koike, T., Calatayud, V., Yuan, X., Liu, X., De Marco,  
535 A., Jolivet, Y., Kontunen-Soppela, S., Hoshika, Y., Saji, H., Li, P., Li, Z., Watanabe, M., and Kobayashi, K.: Emerging challenges of ozone  
536 impacts on asian plants: actions are needed to protect ecosystem health, *Ecosystem Health and Sustainability*, 7, 1911602,  
537 [10.1080/20964129.2021.1911602](https://doi.org/10.1080/20964129.2021.1911602), 2021.

538 [Feng, Z. Z., Sun, J. S., Wan, W. X., Hu, E. Z., and Calatayud, V.: Evidence of widespread ozone-induced visible injury on plants in Beijing,](#)  
539 [China, \*Environ Pollut\*, 193, 296-301, \[10.1016/j.envpol.2014.06.004\]\(https://doi.org/10.1016/j.envpol.2014.06.004\), 2014.](#)

540 Feng, Z. Z., Buker, P., Pleijel, H., Emberson, L., Karlsson, P. E., and Uddling, J.: A unifying explanation for variation in ozone sensitivity  
541 among woody plants, *Glob. Change Biol.*, 24, 78-84, [10.1111/gcb.13824](https://doi.org/10.1111/gcb.13824), 2018.

542 [Fritz, M. A., Rosa, S., and Sicard, A.: Mechanisms Underlying the Environmentally Induced Plasticity of Leaf Morphology, \*Front Genet\*, 9,](#)  
543 [478, \[10.3389/fgene.2018.00478\]\(https://doi.org/10.3389/fgene.2018.00478\), 2018.](#)

544 [Fuhrer, J., Skarby, L., and Ashmore, M. R.: Critical levels for ozone effects on vegetation in Europe, \*Environ Pollut\*, 97, 91-106,](#)  
545 [10.1016/s0269-7491\(97\)00067-5, 1997.](#)

546 [Feng, Z. Z., Sun, J. S., Wan, W. X., Hu, E. Z., and Calatayud, V.: Evidence of widespread ozone-induced visible injury on plants in Beijing,](#)  
547 [China, \*Environ Pollut\*, 193, 296-301, 2014.](#)

548 Fyllas, N. M., Quesada, C. A., and Lloyd, J.: Deriving Plant Functional Types for Amazonian forests for use in vegetation dynamics models,  
549 *Perspectives in Plant Ecology, Evolution and Systematics*, 14, 97-110, 2012-<https://doi.org/10.1016/j.ppees.2011.11.001>, 2012.

550 Gallagher, R. V., Falster, D. S., Maitner, B. S., Salguero-Gomez, R., Vandvik, V., Pearse, W. D., Schneider, F. D., Kattge, J., Poelen, J. H.,  
551 Madin, J. S., Ankenbrand, M. J., Penone, C., Feng, X., Adams, V. M., Alroy, J., Andrew, S. C., Balk, M. A., Bland, L. M., Boyle, B. L.,  
552 Bravo-Avila, C. H., Brennan, I., Carthey, A. J. R., Catullo, R., Cavazos, B. R., Conde, D. A., Chown, S. L., Fadrique, B., Gibb, H., Halbritter,  
553 A. H., Hammock, J., Hogan, J. A., Holewa, H., Hope, M., Iversen, C. M., Jochum, M., Kearney, M., Keller, A., Mabee, P., Manning, P.,  
554 McCormack, L., Michaletz, S. T., Park, D. S., Perez, T. M., Pineda-Munoz, S., Ray, C. A., Rossetto, M., Sauquet, H., Sparrow, B., Spasojevic,  
555 M. J., Telford, R. J., Tobias, J. A., Violle, C., Walls, R., Weiss, K. C. B., Westoby, M., Wright, I. J., and Enquist, B. J.: Open Science  
556 principles for accelerating trait-based science across the Tree of Life, *Nat Ecol Evol*, 4, 294-303, [10.1038/s41559-020-1109-6](https://doi.org/10.1038/s41559-020-1109-6), 2020.

557 Gelaro, R., McCarty, W., Suarez, M. J., Todling, R., Molod, A., Takacs, L., Randles, C. A., Darmenov, A., Bosilovich, M. G., Reichle, R.,  
558 Wargan, K., Coy, L., Cullather, R., Draper, C., Akella, S., Buchard, V., Conaty, A., da Silva, A. M., Gu, W., Kim, G.-K., Koster, R., Lucchesi,  
559 R., Merkova, D., Nielsen, J. E., Partyka, G., Pawson, S., Putman, W., Rienecker, M., Schubert, S. D., Sienkiewicz, M., and Zhao, B.: The  
560 Modern-Era Retrospective Analysis for Research and Applications, Version 2 (MERRA-2), *J Climate*, 30, 5419-5454, [10.1175/jcli-d-16-](https://doi.org/10.1175/jcli-d-16-0758.1)  
561 [0758.1](#), 2017.

562 [Gong, C., Lei, Y., Ma, Y., Yue, X., and Liao, H.: Ozone-vegetation feedback through dry deposition and isoprene emissions in a global](#)  
563 [chemistry-carbon-climate model, \*Atmos. Chem. Phys.\*, 20, 3841-3857, \[10.5194/acp-20-3841-2020\]\(https://doi.org/10.5194/acp-20-3841-2020\), 2020.](#)

564 [Gong, C., Liao, H., Yue, X., Ma, Y., and Lei, Y.: Impacts of Ozone-Vegetation Interactions on Ozone Pollution Episodes in North China](#)  
565 [and the Yangtze River Delta, \*Geophys Res Lett\*, 48, \[10.1029/2021gl093814\]\(https://doi.org/10.1029/2021gl093814\), 2021.](#)

566 Henry, C., John, G. P., Pan, R., Bartlett, M. K., Fletcher, L. R., Scoffoni, C., and Sack, L.: A stomatal safety-efficiency trade-off constrains  
567 responses to leaf dehydration, *Nat Commun*, 10, 3398, [10.1038/s41467-019-11006-1](https://doi.org/10.1038/s41467-019-11006-1), 2019.

568 Herdt, R. W.: The state of food and agriculture, 2003-2004: Agricultural biotechnology: Meeting the needs of the poor?, *Agricultural*  
569 *Economics*, 32, 109-+, 2005-[10.1111/j.0169-5150.2005.t01-7-00008.x](https://doi.org/10.1111/j.0169-5150.2005.t01-7-00008.x), 2005.

570 [Kattge, J., Hong, C., Mueller, N. D., Burney, J. A., Zhang, Y., AghaKouchak, A., Moore, F. C., Qin, Y., Tong, D., and Davis, S. J.: Impacts](#)  
571 [of ozone and climate change on yields of perennial crops in California, \*Nature Food\*, 1, 166-172, \[10.1038/s43016-020-0043-8\]\(https://doi.org/10.1038/s43016-020-0043-8\), 2020.](#)

572 [Kattge, J., Diaz, S., and Lavorel, S., and Prentice, I. C., and Leadley, P., and Bonisch, G., and Garnier, E., and Westoby, M., and Reich,](#)  
573 [P. B., and Wright, I. J., and Cornelissen, J. H. C., and Violle, C., and Harrison, S. P., and van Bodegom, P. M., and Reichstein, M., and](#)  
574 [Enquist, B. J., and Soudzilovskaia, N. A., and Ackerly, D. D., and Anand, M., and Atkin, O., and Bahn, M., and Baker, T. R., and](#)  
575 [Baldocchi, D., and Bekker, R., and Blanco, C. C., and Blonder, B., and Bond, W. J., and Bradstock, R., and Bunker, D. E., and Casanoves,](#)  
576 [F., and Cavender-Bares, J., and Chambers, J. Q., and Chapin, F. S., and Chave, J., and Coomes, D., and Cornwell, W. K., and Craine, J.](#)  
577 [M., and Dobrin, B. H., and Duarte, L., and Durka, W., and Elser, J., and Esser, G., and Estiarte, M., and Fagan, W. F., and Fang, J., and](#)  
578 [Fernandez-Mendez, F., and Fidelis, A., and Finegan, B., and Flores, O., and Ford, H., and Frank, D., and Freschet, G. T., and Fyllas, N.](#)  
579 [M., and Gallagher, R. V., and Green, W. A., and Gutierrez, A. G., and Hickler, T., and Higgins, S. I., and Hodgson, J. G., and Jalili, A.,](#)  
580 [and Jansen, S., and Joly, C. A., and Kerkhoff, A. J., and Kirkup, D., and Kitajima, K., and Kleyer, M., and Klotz, S., and Knops, J. M.](#)  
581 [H., and Kramer, K., and Kuhn, I., and Kurokawa, H., and Laughlin, D., and Lee, T. D., and Leishman, M., and Lens, F., and Lenz, T.,](#)

582 [and](#), Lewis, S. L. [and](#), Lloyd, J. [and](#), Llusia, J. [and](#), Louault, F. [and](#), Ma, S. [and](#), Mahecha, M. D. [and](#), Manning, P. [and](#), Massad, T. [and](#),  
583 Medlyn, B. E. [and](#), Messier, J. [and](#), Moles, A. T. [and](#), Muller, S. C. [and](#), Nadrowski, K. [and](#), Naeem, S. [and](#), Niinemets, U. [and](#), Nollert,  
584 S. [and](#), Nuske, A. [and](#), Ogaya, R. [and](#), Oleksyn, J. [and](#), Onipchenko, V. G. [and](#), Onoda, Y. [and](#), Ordonez, J. [and](#), Overbeck, G. [and](#),  
585 Ozinga, W. A. [and](#), Patino, S. [and](#), Paula, S. [and](#), Pausas, J. G. [and](#), Penuelas, J. [and](#), Phillips, O. L. [and](#), Pillar, V. [and](#), Poorter, H. [and](#),  
586 Poorter, L. [and](#), Poschlod, P. [and](#), Prinzing, A. [and](#), Proulx, R. [and](#), Rammig, A. [and](#), Reinsch, S. [and](#), Reu, B. [and](#), Sack, L. [and](#),  
587 Salgado-Negre, B. [and](#), Sardans, J. [and](#), Shiodera, S. [and](#), Shipley, B. [and](#), Siefert, A. [and](#), Sosinski, E. [and](#), Soussana, J. F. [and](#), Swaine,  
588 E. [and](#), Swenson, N. [and](#), Thompson, K. [and](#), Thornton, P. [and](#), Waldram, M. [and](#), Weiher, E. [and](#), White, M. [and](#), White, S. [and](#), Wright,  
589 S. J. [and](#), Yguel, B. [and](#), Zaehle, S. [and](#), Zanne, A. E. [and](#) Wirth, C.: TRY - a global database of plant traits, *Global Change Biol*, 17,  
590 2905-2935, [Doi 10.1111/J.1365-2486.2011.02451.X](#), 2011.  
591 [Keenan, T. F. and Niinemets, U.: Global leaf trait estimates biased due to plasticity in the shade, \*Nat Plants\*, 3, ARTN 16201](#)  
592 [10.1038/nplants.2016.201](#), 2017.  
593 [Kochhar, S. and Gujral, S.: Abiotic and Biotic Stress, in: \*Plant Physiology: Theory and Applications\*, 2 ed., edited by: Kochhar, S. L., and](#)  
594 [Gujral, S. K., Cambridge University Press, Cambridge, 545-589, DOI: 10.1017/9781108486392.021](#), 2020.  
595 Li, D., Wang, X., Zheng, H., Zhou, K., Yao, X., Tian, Y., Zhu, Y., Cao, W., and Cheng, T.: Estimation of area- and mass-based leaf nitrogen  
596 contents of wheat and rice crops from water-removed spectra using continuous wavelet analysis, *Plant Methods*, 14, [10.1186/s13007-018-](#)  
597 [0344-1](#), 2018.  
598 Li, P., Calatayud, V., Gao, F., Uddling, J., and Feng, Z. Z.: Differences in ozone sensitivity among woody species are related to leaf  
599 morphology and antioxidant levels, *Tree Physiol.*, 36, 1105-1116, [10.1093/treephys/tpw042](#), 2016.  
600 Li, P., Feng, Z., Calatayud, V., Yuan, X., Xu, Y., and Paoletti, E.: A meta-analysis on growth, physiological, and biochemical responses of  
601 woody species to ground-level ozone highlights the role of plant functional types, *Plant Cell Environ*, 40, 2369-2380, [10.1111/pce.13043](#),  
602 2017.  
603 Li, S., Moller, C. A., Mitchell, N. G., Lee, D., Sacks, E. J., and Ainsworth, E. A.: Testing unified theories for ozone response in C-4 species,  
604 *Global Change Biol*, 28, 3379-3393, [10.1111/gcb.16108](#), 2022.  
605 Lombardozzi, D., Levis, S., Bonan, G., Hess, P. G., and Sparks, J. P.: The Influence of Chronic Ozone Exposure on Global Carbon and  
606 Water Cycles, *J Climate*, 28, 292-305, [10.1175/Jcli-D-14-00223.1](#), 2015.  
607 Massman, W. J., Musselman, R. C., and Lefohn, A. S.: A conceptual ozone dose-response model to develop a standard to protect vegetation,  
608 *Atmos Environ*, 34, 745-759, [10.1016/s1352-2310\(99\)00395-7](#), 2000.  
609 [Mills, G., Hayes, F., Simpson, D., Emberson, L., Norris, D., Harmens, H., and Buker, P.: Evidence of widespread effects of ozone on crops](#)  
610 [and \(semi-\)natural vegetation in Europe \(1990-2006\) in relation to AOT40-and flux-based risk maps, \*Global Change Biol\*, 17, 592-613,](#)  
611 [10.1111/j.1365-2486.2010.02217.x](#), 2011.  
612 [Mills, G., Sharps, K., Simpson, D., Pleijel, H., Frei, M., Burkey, K., Emberson, L., Uddling, J., Broberg, M., Feng, Z., Kobayashi, K., and](#)  
613 [Agrawal, M.: Closing the global ozone yield gap: Quantification and cobenefits for multistress tolerance, \*Glob Chang Biol\*, 24, 4869-4893,](#)  
614 [10.1111/gcb.14381](#), 2018a.  
615 Mills, G., Sharps, K., Simpson, D., Pleijel, H., Broberg, M., Uddling, J., Jaramillo, F., Davies, W. J., Dentener, F., Van den Berg, M.,  
616 Agrawal, M., Agrawal, S. B., Ainsworth, E. A., Buker, P., Emberson, L., Feng, Z. Z., Harmens, H., Hayes, F., Kobayashi, K., Paoletti, E.,  
617 and Van Dingenen, R.: Ozone pollution will compromise efforts to increase global wheat production, *Global Change Biol*, 24, 3560-3574,  
618 [2018a](#)[10.1111/gcb.14157](#), 2018b.  
619 ~~[Mills, G., Sharps, K., Simpson, D., Pleijel, H., Frei, M., Burkey, K., Emberson, L., Uddling, J., Broberg, M., Feng, Z., Kobayashi, K., and](#)~~  
620 ~~[Agrawal, M.: Closing the global ozone yield gap: Quantification and cobenefits for multistress tolerance, \*Glob Chang Biol\*, 24, 4869-4893,](#)~~  
621 ~~[2018b.](#)~~  
622 Moreno-Martinez, A., Camps-Valls, G., Kattge, J., Robinson, N., Reichstein, M., van Bodegom, P., Kramer, K., Cornelissen, J. H. C., Reich,  
623 P., Bahn, M., Niinemets, U., Penuelas, J., Craine, J. M., Cerabolini, B. E. L., Minden, V., Laughlin, D. C., Sack, L., Allred, B., Baraloto, C.,  
624 Byun, C., Soudzilovskaia, N. A., and Running, S. W.: A methodology to derive global maps of leaf traits using remote sensing and climate  
625 data, *Remote Sens Environ*, 218, 69-88, 2018.  
626 Mukherjee, A., Yadav, D. S., Agrawal, S. B., and Agrawal, M.: Ozone a persistent challenge to food security in India: Current status and  
627 policy implications, *Current Opinion in Environmental Science & Health*, 19, 100220, [2021-https://doi.org/10.1016/j.coesh.2020.10.008](#),  
628 2021.  
629 [Oliver, R. J., Mercado, L. M., Sitch, S., Simpson, D., Medlyn, B. E., Lin, Y. S., and Folberth, G. A.: Large but decreasing effect of ozone](#)  
630 [on the European carbon sink, \*Biogeosciences\*, 15, 4245-4269, 10.5194/bg-15-4245-2018](#), 2018.  
631 [Ollinger, S. V., Aber, J. D., and Reich, P. B.: Simulating Ozone Effects on Forest Productivity: Interactions among Leaf-, Canopy-, and](#)  
632 [Stand-Level Processes, \*Ecol Appl\*, 7, 1237-1251, 10.2307/2641211](#), 1997.  
633 [Peng, J. L., Shang, B., Xu, Y. S., Feng, Z. Z., Pleijel, H., and Calatayud, V.: Ozone exposure- and flux-yield response relationships for maize,](#)  
634 [\*Environ Pollut\*, 252, 1-7](#), 2019.  
635 Poorter, H., Niinemets, U., Poorter, L., Wright, I. J., and Villar, R.: Causes and consequences of variation in leaf mass per area (LMA): a  
636 meta-analysis, *New Phytol*, 182, 565-588, [10.1111/j.1469-8137.2009.02830.x](#), 2009.



637 Reich, P. B.: The world-wide 'fast-slow' plant economics spectrum: a traits manifesto, *J Ecol*, 102, 275-301, [10.1111/1365-2745.12211](https://doi.org/10.1111/1365-2745.12211),  
638 2014.

639 Reich, P. B. and Amundson, R. G.: AMBIENT LEVELS OF OZONE REDUCE NET PHOTOSYNTHESIS IN TREE AND CROP  
640 SPECIES, *Science*, 230, 566-570, [10.1126/science.230.4725.566](https://doi.org/10.1126/science.230.4725.566), 1985.

641 Reich, P. B., Ellsworth, D. S., and Walters, M. B.: Leaf structure (specific leaf area) modulates photosynthesis-nitrogen relations: evidence  
642 from within and across species and functional groups, *Funct Ecol*, 12, 948-958, [1998-DOI 10.1046/j.1365-2435.1998.00274.x](https://doi.org/10.1046/j.1365-2435.1998.00274.x), 1998.

643 [Reich, P. B., Walters, M. B., and Ellsworth, D. S.: From tropics to tundra: Global convergence in plant functioning, \*P Natl Acad Sci USA\*,  
644 94, 13730-13734, 10.1073/pnas.94.25.13730, 1997.](https://doi.org/10.1073/pnas.94.25.13730)

645 Reich, P. B., Ellsworth, D. S., Walters, M. B., Vose, J. M., Gresham, C., Volin, J. C., and Bowman, W. D.: Generality of leaf trait  
646 relationships: A test across six biomes, *Ecology*, 80, 1955-1969, [1999-10.1890/0012-9658\(1999\)080\[1955:goltra\]2.0.co;2](https://doi.org/10.1890/0012-9658(1999)080[1955:goltra]2.0.co;2), 1999.

647 [Reich, P. B., Walters, M. B., and Ellsworth, D. S.: From tropics to tundra: Global convergence in plant functioning, \*P Natl Acad Sci USA\*,  
648 94, 13730-13734, 1997.](https://doi.org/10.1073/pnas.94.25.13730)

649 Richards, B. L., Middleton, J. T., and Hewitt, W. B.: Air Pollution With Relation to Agronomic Crops: V. Oxidant Stipple of Grape, *Agron*  
650 *J*, 50, 559-561, 1958.

651 Richards, R. A.: Selectable traits to increase crop photosynthesis and yield of grain crops, *J Exp Bot*, 51, 447-458,  
652 [10.1093/jexbot/51.suppl\\_1.447](https://doi.org/10.1093/jexbot/51.suppl_1.447), 2000.

653 [Shang, B., Feng, Z. Z., Li, P., Yuan, X. Y., Xu, Y. S., and Calatayud, V.: Ozone exposure- and flux-based response relationships with  
654 photosynthesis, leaf morphology and biomass in two poplar clones, \*Sci Total Environ\*, 603, 185-195, 10.1016/j.scitotenv.2017.06.083, 2017.](https://doi.org/10.1016/j.scitotenv.2017.06.083)

655 Shipley, B., Lechowicz, M. J., Wright, I., and Reich, P. B.: Fundamental trade-offs generating the worldwide leaf economics spectrum,  
656 *Ecology*, 87, 535-541, [10.1890/05-1051](https://doi.org/10.1890/05-1051), 2006.

657 Sitch, S., Cox, P. M., Collins, W. J., and Huntingford, C.: Indirect radiative forcing of climate change through ozone effects on the land-  
658 carbon sink, *Nature*, 448, 791-794, [10.1038/Nature06059](https://doi.org/10.1038/Nature06059), 2007.

659 [Tai, A. P. K., Martin, M. V., and Heald, C. L.: Threat to future global food security from climate change and ozone air pollution, \*Nat Clim  
660 Change\*, 4, 817-821, 10.1038/nclimate2317, 2014.](https://doi.org/10.1038/nclimate2317)

661 [Tai, A. P. K., Sadiq, M., Pang, J. Y. S., Yung, D. H. Y., and Feng, Z.: Impacts of Surface Ozone Pollution on Global Crop Yields: Comparing  
662 Different Ozone Exposure Metrics and Incorporating Co-effects of CO<sub>2</sub>, \*Frontiers in Sustainable Food Systems\*, 5,  
663 10.3389/fsufs.2021.534616, 2021.](https://doi.org/10.3389/fsufs.2021.534616)

664 Tiwari, S., Grote, R., Churkina, G., and Butler, T.: Ozone damage, detoxification and the role of isoprenoids - new impetus for integrated  
665 models, *Funct Plant Biol*, 43, 324-336, [10.1071/fp15302](https://doi.org/10.1071/fp15302), 2016.

666 Turnock, S. T., Wild, O., Dentener, F. J., Davila, Y., Emmons, L. K., Flemming, J., Folberth, G. A., Henze, D. K., Jonson, J. E., Keating, T.  
667 J., Kengo, S., Lin, M., Lund, M., Tilmes, S., and O'Connor, F. M.: The impact of future emission policies on tropospheric ozone using a  
668 parameterised approach, *Atmos Chem Phys*, 18, 8953-8978, [10.5194/acp-18-8953-2018](https://doi.org/10.5194/acp-18-8953-2018), 2018.

669 [Walker, A. P., Beckerman, A. P., Gu, L., Kattge, J., Cernusak, L. A., Domingues, T. F., Scales, J. C., Wohlfahrt, G., Wullschlegel, S. D.,  
670 and Woodward, F. I.: The relationship of leaf photosynthetic traits – V<sub>cmax</sub> and J<sub>max</sub> – to leaf nitrogen, leaf phosphorus, and specific leaf  
671 area: a meta-analysis and modeling study, \*Ecol Evol\*, 4, 3218-3235, <https://doi.org/10.1002/ece3.1173>, 2014.](https://doi.org/10.1002/ece3.1173)

672 Wang, K. and Shangguan, Z.: Photosynthetic characteristics and resource utilization efficiency of maize (*Zea mays*L.) and millet (*Setaria*  
673 *italica*L.) in a semi-arid hilly loess region in China, *New Zeal J Crop Hort*, 38, 247-254, [10.1080/01140671.2010.503987](https://doi.org/10.1080/01140671.2010.503987), 2010.

674 Wittig, V. E., Ainsworth, E. A., Naidu, S. L., Karnosky, D. F., and Long, S. P.: Quantifying the impact of current and future tropospheric  
675 ozone on tree biomass, growth, physiology and biochemistry: a quantitative meta-analysis, *Global Change Biol*, 15, 396-424, 2009.

676 Wright, I. J., Westoby, M., and Reich, P. B.: Convergence towards higher leaf mass per area in dry and nutrient-poor habitats has different  
677 consequences for leaf life span, *J Ecol*, 90, 534-543, [10.1046/j.1365-2745.2002.00689.x](https://doi.org/10.1046/j.1365-2745.2002.00689.x), 2002.

678 [Wright, I. J., Reich, P. B., Cornelissen, J. H. C., Falster, D. S., Groom, P. K., Hikosaka, K., Lee, W., Lusk, C. H., Niinemets, U., Oleksyn,  
679 J., Osada, N., Poorter, H., Warton, D. L., and Westoby, M.: Modulation of leaf economic traits and trait relationships by climate, \*Global Ecol  
680 Biogeogr\*, 14, 411-421, 10.1111/j.1466-822x.2005.00172.x, 2005.](https://doi.org/10.1111/j.1466-822x.2005.00172.x)

681 Wu, Y., Gong, W., Wang, Y., Yong, T., Yang, F., Liu, W., Wu, X., Du, J., Shu, K., Liu, J., Liu, C., and Yang, W.: Leaf area and  
682 photosynthesis of newly emerged trifoliolate leaves are regulated by mature leaves in soybean, *J Plant Res*, 131, 671-680, [10.1007/s10265-  
683 018-1027-8](https://doi.org/10.1007/s10265-018-1027-8), 2018.

684 Yue, X. and Unger, N.: The Yale Interactive terrestrial Biosphere model version 1.0: description, evaluation and implementation into NASA  
685 GISS ModelE2, *Geosci Model Dev*, 8, 2399-2417, [10.5194/gmd-8-2399-2015](https://doi.org/10.5194/gmd-8-2399-2015), 2015.

686 [Yue, X. and Unger, N.: Fire air pollution reduces global terrestrial productivity, \*Nat Commun\*, 9, 5413, 2018.](https://doi.org/10.1016/j.sciadv.2021.1620)

687 Zalles, V., Hansen, M. C., Potapov, P. V., Parker, D., Stehman, S. V., Pickens, A. H., Parente, L. L., Ferreira, L. G., Song, X.-P., Hernandez-  
688 Serna, A., and Kommareddy, I.: Rapid expansion of human impact on natural land in South America since 1985, *Sci Adv*, 7, eabg1620,  
689 [10.1126/sciadv.abg1620](https://doi.org/10.1126/sciadv.abg1620), 2021.

690 [Zhou, S. S., Tai, A. P. K., Sun, S., Sadiq, M., Heald, C. L., and Geddes, J. A.: Coupling between surface ozone and leaf area index in a  
691 chemical transport model: strength of feedback and implications for ozone air quality and vegetation health, \*Atmos. Chem. Phys.\*, 18, 14133-  
692 14148, 10.5194/acp-18-14133-2018, 2018.](https://doi.org/10.5194/acp-18-14133-2018)

693 [Zhu, J., Tai, A. P. K., and Hung Lam Yim, S.: Effects of ozone–vegetation interactions on meteorology and air quality in China using a two-](#)  
694 [way coupled land–atmosphere model, Atmos. Chem. Phys., 22, 765–782, 10.5194/acp-22-765-2022, 2022.](#)  
695  
696  
697  
698  
699  
700  
701  
702  
703

| 704

| 705

706 **Table 1.** Summary of simulations.

707

Experiment <sup>a</sup>	Method	Thresholds <sup>a</sup> ( <i>x</i> or <i>y</i> )	LMA format	LMA map	Optimal ( <i>a</i> or <i>a<sub>PFT</sub></i> )	Tests ( <i>a</i> or <i>a<sub>PFT</sub></i> )
YIBs-LMA		<i>x</i> =0.019	gridded	M2018	<i>a</i> =3.5 (Table <a href="#">S32</a> )	five tests ( <i>a</i> =2.5, 3, 3.5, 4, 4.5)
YIBs-LMA_PFT	Mass- based	<i>x</i> =0.019	PFT- specific	M2018	<i>a</i> =2.0 (Table <a href="#">S4S3</a> )	five tests ( <i>a</i> =2, 2.5, 3, 3.5, 4)
YIBs-LMA_T		<i>x</i> =0.006	gridded	M2018	<i>a</i> =3.0 (Table <a href="#">S5S4</a> )	five tests ( <i>a</i> =2, 2.5, 3, 3.5, 4)
YIBs-LMA_B2017		<i>x</i> =0.019	gridded	B2017	<i>a</i> =2.8 (Table <a href="#">S6S5</a> )	five tests ( <i>a</i> =2, 2.5, 2.8, 3, 3.5)
YIBs-S2007_adj	Area- based	8 values for <i>y</i> (Table <a href="#">S7S6</a> )	/	/	8 values for <i>a<sub>PFT</sub></i> (Table <a href="#">S7S6</a> )	40 tests (five each for 8 PFTs)

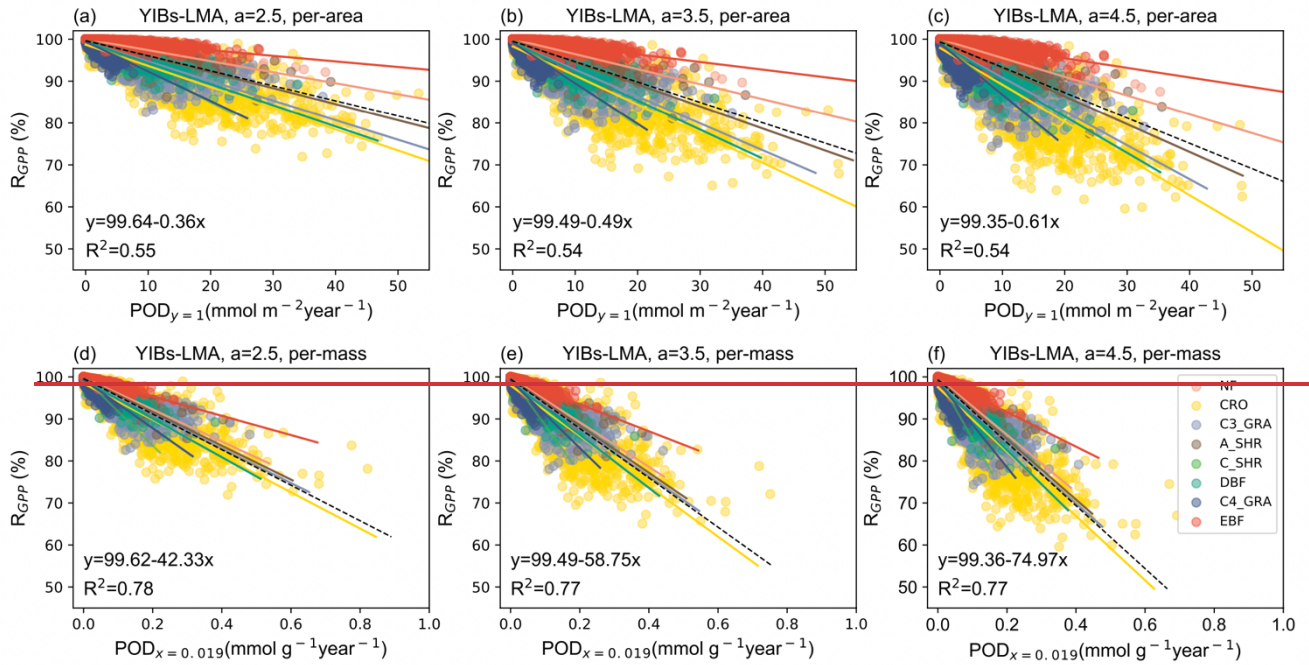
708

709 <sup>a</sup> Units of thresholds are nmol g<sup>-1</sup> s<sup>-1</sup> for *x* and nmol m<sup>-2</sup> s<sup>-1</sup> for *y*710 <sup>b</sup> Units of key parameters are nmol<sup>-1</sup> s g for *a* and nmol<sup>-1</sup> m<sup>2</sup> s for *a<sub>PFT</sub>*

711

712

713



714

715 **Figure 1. Area Table 2. Calibrations of the YIBs-LMA<sup>a</sup> experiment with varied  $a$ .**

716

PFT	$S_o$						$S_s/S_o^b$				
		$a=2.5$	$a=3.0$	$a=3.5$	$a=4.0$	$a=4.5$	$a=2.5$	$a=3.0$	$a=3.5$	$a=4.0$	$a=4.5$
EBF	-0.19	-0.13	-0.16	<b>-0.18</b>	-0.21	-0.23	0.70	0.83	<b>0.96</b>	1.08	1.20
NF	-0.23	-0.26	-0.31	<b>-0.36</b>	-0.40	-0.45	*	*	*	*	*
DBF	-0.70	-0.51	-0.60	<b>-0.69</b>	-0.78	-0.87	0.72	0.86	<b>0.99</b>	1.12	1.24
C_SHR	/	-0.75	-0.90	<b>-1.04</b>	-1.18	-1.31	/	/	/	/	/
A_SHR	/	-0.38	-0.45	<b>-0.53</b>	-0.60	-0.66	/	/	/	/	/
C4_GRA	-0.85	-0.71	-0.84	<b>-0.97</b>	-1.10	-1.22	0.83	0.99	<b>1.14</b>	1.29	1.44
C3_GRA	-0.62	-0.47	-0.55	<b>-0.64</b>	-0.73	-0.81	0.75	0.89	<b>1.03</b>	1.17	1.30
CRO	-3.35	-1.97	-2.57	<b>-3.28</b>	-4.11	-5.10	0.59	0.77	<b>0.98</b>	1.23	1.52
Fitting <sup>c</sup>	/	0.61	0.79	<b>0.99</b>	1.23	1.50	/	/	/	/	/

<u>Median</u>	<u>/</u>	<u>/</u>	<u>/</u>	<u>/</u>	<u>/</u>	<u>/</u>	<u>0.74</u>	<u>0.88</u>	<b><u>1.01</u></b>	<u>1.20</u>	<u>1.37</u>
							<u>(0.72)</u>	<u>(0.86)</u>	<b><u>(0.99)</u></b>	<u>(1.17)</u>	<u>(1.30)</u>
<u>Std</u>	<u>/</u>	<u>/</u>	<u>/</u>	<u>/</u>	<u>/</u>	<u>/</u>	<u>0.19</u>	<u>0.21</u>	<b><u>0.23</u></b>	<u>0.25</u>	<u>0.28</u>
							<u>(0.09)</u>	<u>(0.08)</u>	<b><u>(0.07)</u></b>	<u>(0.08)</u>	<u>(0.13)</u>

717

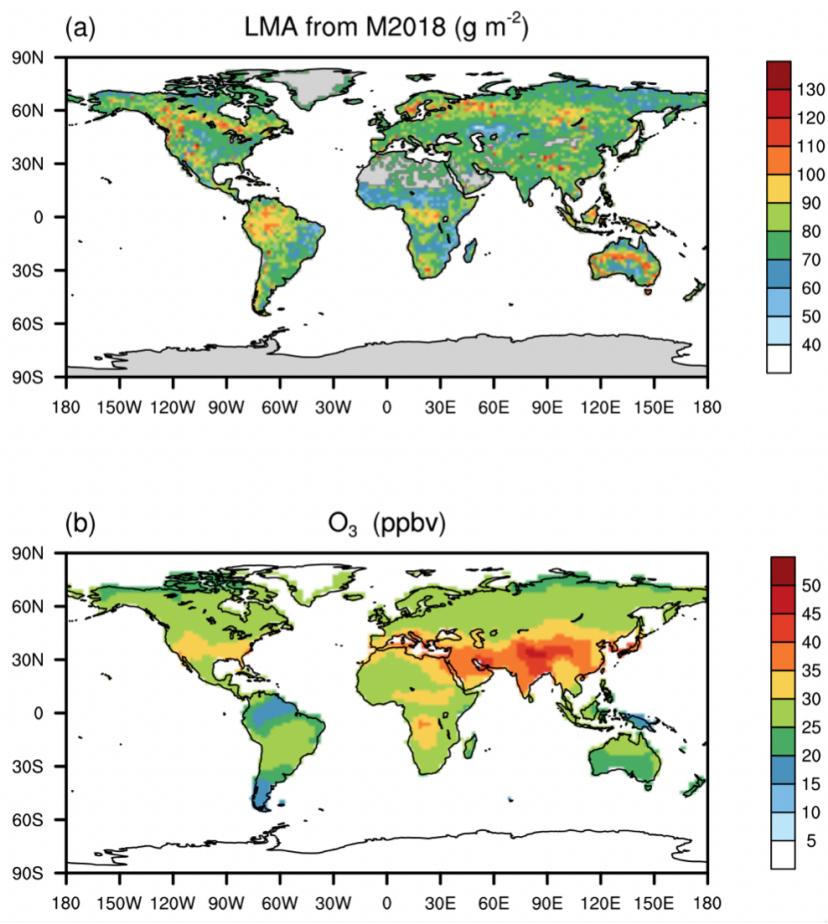
718 <sup>a</sup> All runs from the YIBs-LMA experiment use  $x=0.019 \text{ nmol g}^{-1} \text{ s}^{-1}$  and LMA map from M2018.

719 <sup>b</sup> Slopes of simulated DRRs ( $S_S$ ) are divided by observations ( $S_O$ , Table S1) to derive the model-to-observation ratios (" $S_S/S_O$ ").

720  $O_3$  dose metric is  $POD_{y=1}$  for natural PFTs and  $POD_{y=6}$  for crops. The Median and standard deviation (Std) of  $S_S/S_O$  ratios of  
 721 all PFTs are calculated for each set of specific parameter  $a$ . The values in parentheses exclude the effect of those numbers  
 722 marked with \* that are out of 1 standard deviation.

723 <sup>c</sup> The slopes (Fitting) of linear regressions between  $S_O$  and  $S_S$  are listed for each  $a$ . The optimal  $a$  with 1:1 fitting between  $S_S$   
 724 and  $S_O$  is bolded.

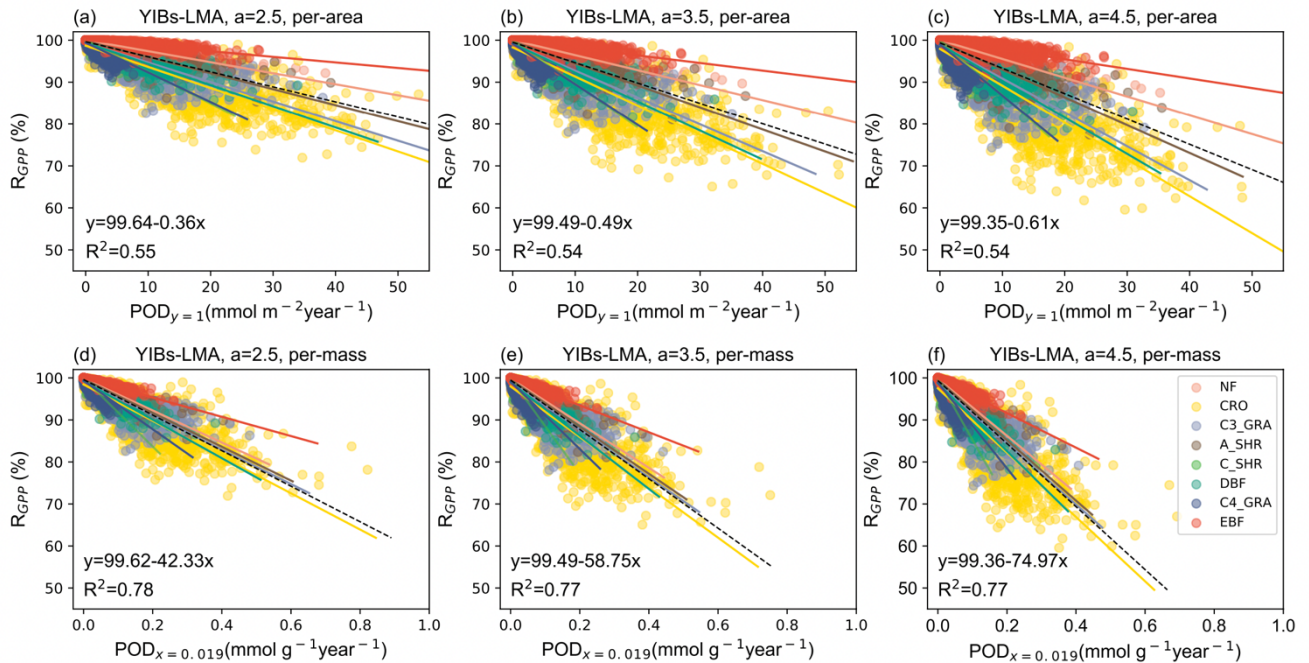
725



726

727 **Figure 1.** Global leaf mass per area (LMA) and surface ozone (O<sub>3</sub>) concentrations. The (a) LMA is  
728 adopted from Moreno-Martinez et al. (2018) (M2018) and (b) annual mean O<sub>3</sub> is derived from TF-HTAP  
729 (Turnock et al., 2018).

730

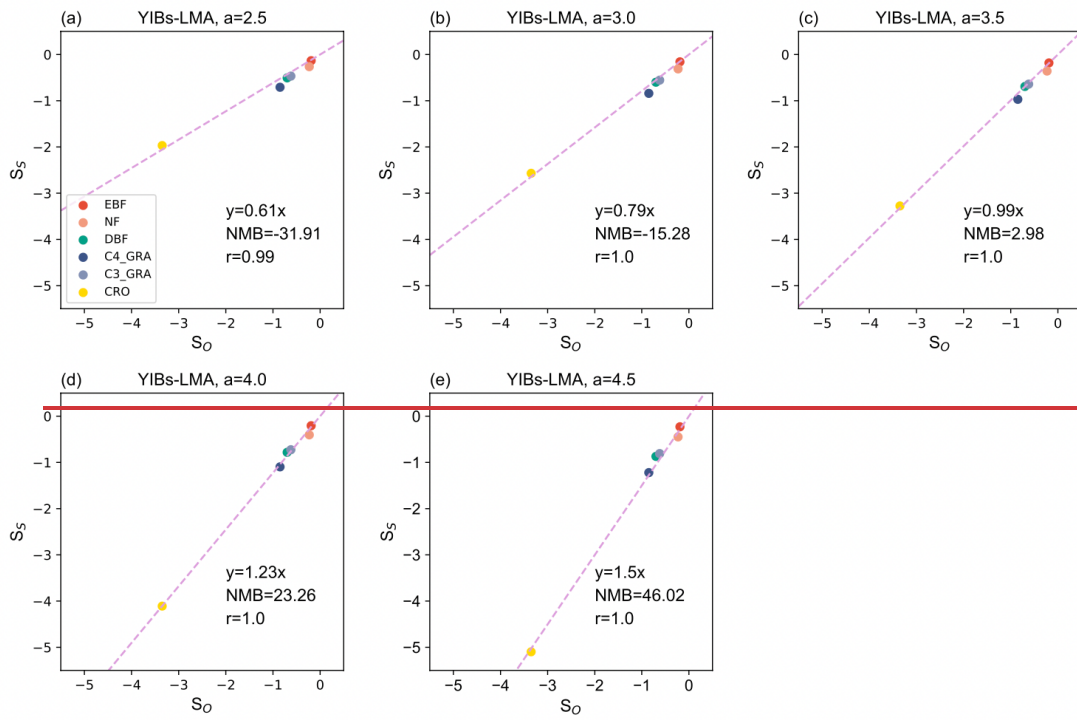


732

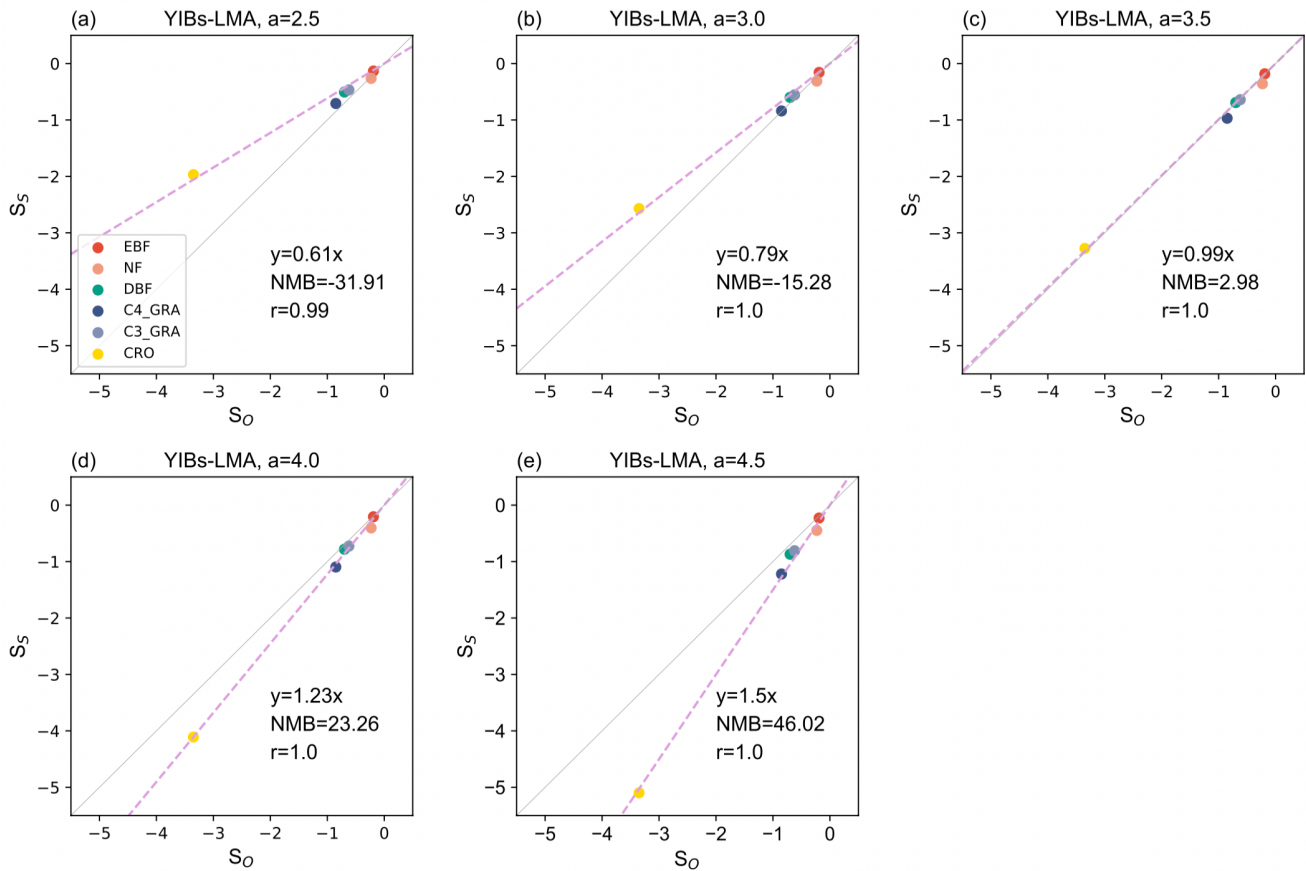
733 **Figure 2.** Simulated area-based (top) or mass-based (bottom) DRRs for the YIBs-LMA experiment.  
 734 Three tests from the YIBs-LMA experiment all adopt  $x=0.019 \text{ nmol g}^{-1} \text{ s}^{-1}$  and gridded LMA from M2018  
 735 with parameter  $a=2.5, 3.5, 4.5 \text{ nmol}^{-1} \text{ s g}$ , respectively. Each dot represents estimated POD- $R_{GPP}$  ( $\text{POD}_{y=1}$   
 736 for (a)-(c),  $\text{POD}_{x=0.019}$  for (d)-(e)) at a grid with corresponding PFT. The PFT-specific regressions between  
 737 area- or mass- based POD and  $R_{GPP}$  are displayed with solid lines shown in legend. Regression  
 738 relationships of all PFTs are displayed in black dash line with coefficients of determination ( $R^2$ ) denoted  
 739 on each panel. Note the differences of ranges in x axis among PFTs. The YIBs-LMA experiment is  
 740 summarized in Table 1.

741





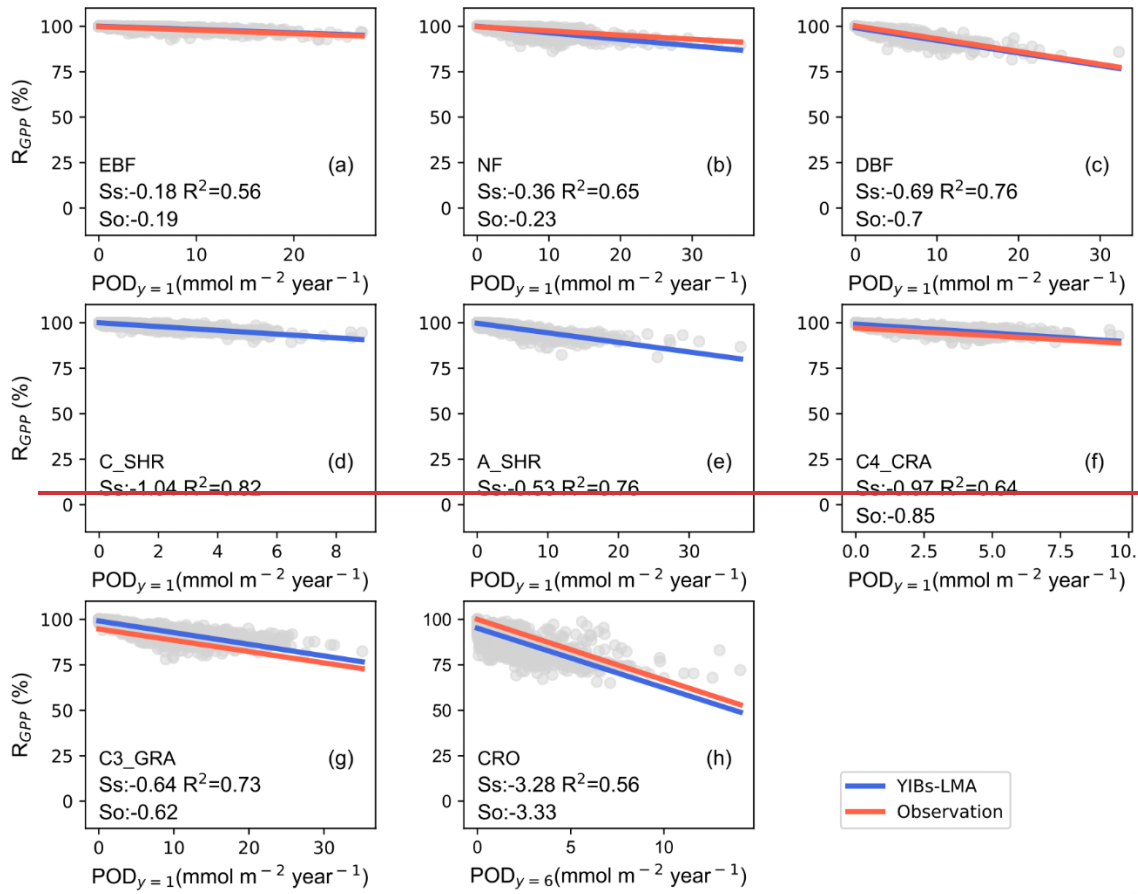
742



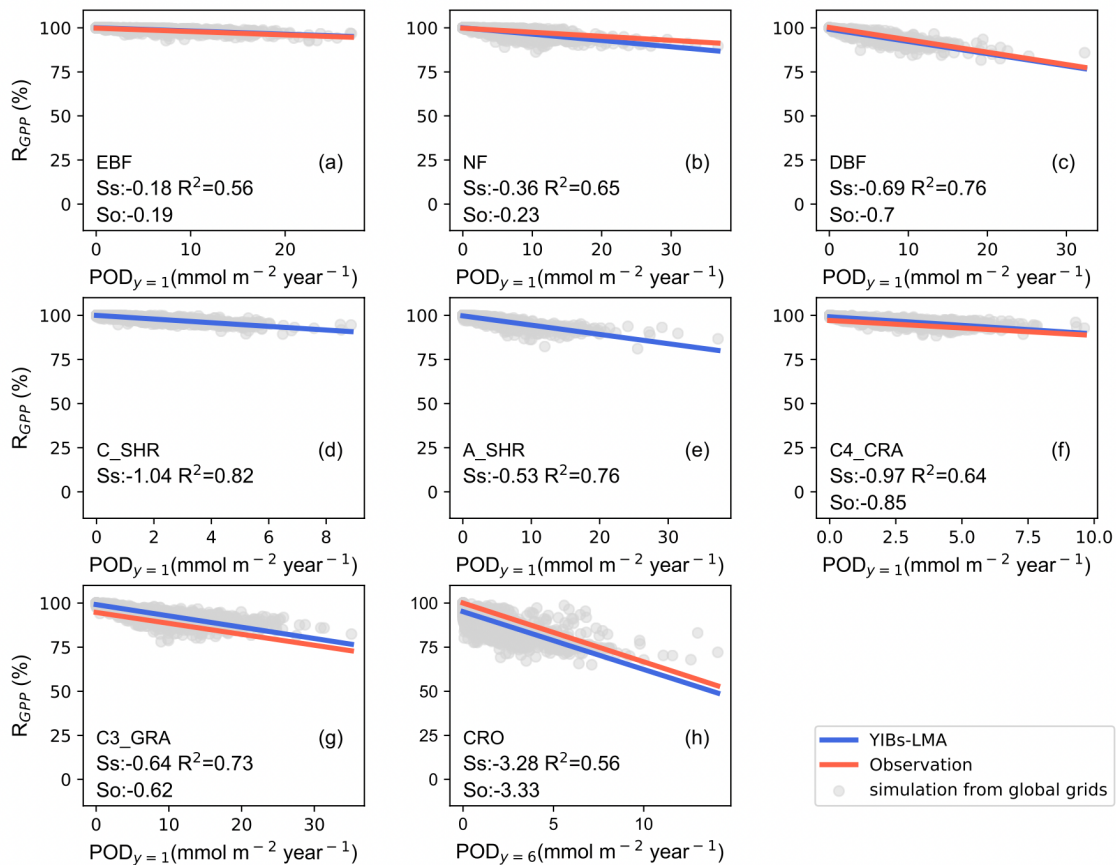
743

744 **Figure 23.** Comparison between  $S_O$  (% per  $\text{mmol m}^{-2}$ ) and  $S_S$  (% per  $\text{mmol m}^{-2}$ ) for the YIBs-LMA  
 745 experiment. Five tests from the YIBs-LMA experiment all adopt  $x=0.019 \text{ nmol g}^{-1} \text{ s}^{-1}$  and gridded LMA  
 746 from M2018 but with varied parameter  $a$  from (a) 2.5 to (e) 4.5  $\text{nmol}^{-1} \text{ s g}$ .  $S_O$  are from Table S1.  $S_S$  are  
 747 derived as the slope between  $R_{\text{GPP}}$  and  $\text{POD}_y$ . The linear regression (dashed lines), 1:1 fitting (light grey  
 748 lines), normalized mean biases (NMB), and correlation coefficient ( $r$ ) between  $S_S$  and  $S_O$  for varied PFTs  
 749 are shown on each panel. The  $S_S$  and  $S_O$  of CRO are derived using  $\text{POD}_{y=6}$  while other PFTs use  $\text{POD}_{y=1}$ .  
 750 The YIBs-LMA experiment is described in Table 1.

751

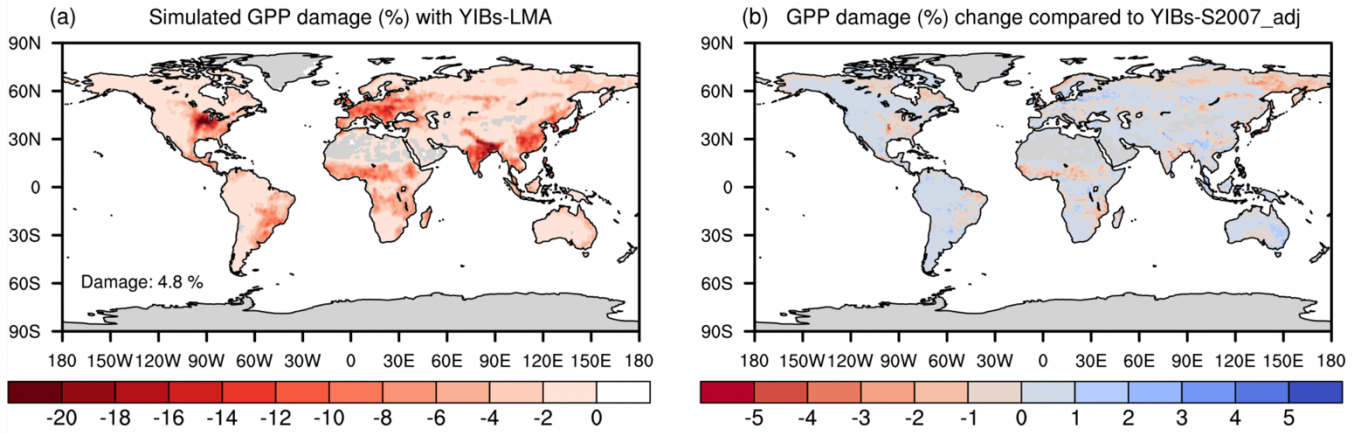


752



753

754 **Figure 34.** Comparisons of observed and simulated dose-response relationships. Simulated PFT-specific  
755 DRRs are derived from YIBs-LMA with gridded LMA from M2018,  $x=0.019 \text{ nmol g}^{-1} \text{ s}^{-1}$ , and  $\alpha=3.5$   
756  $\text{nmol}^{-1} \text{ s g}$ . Each dot represents results from a gridcell with corresponding PFT. The regressions between  
757 relative GPP percentage ( $R_{GPP}$ ) and leaf area-based stomatal  $O_3$  uptake fluxes ( $POD_{y=1}$  for natural PFTs  
758 and  $POD_{y=6}$  for crops) are shown for observations (red, see Table S1) and simulations (blue) with slopes  
759 of DRRs denoted as  $S_o$  and  $S_s$ , respectively.  $S_o$  are missing for (d) cold and (e) arid shrubs. Coefficients  
760 of determination ( $R^2$ ) of simulations are displayed in each panel. Note the differences of ranges in x axis  
761 among PFTs (PFTs are shown in Fig. S2S1).

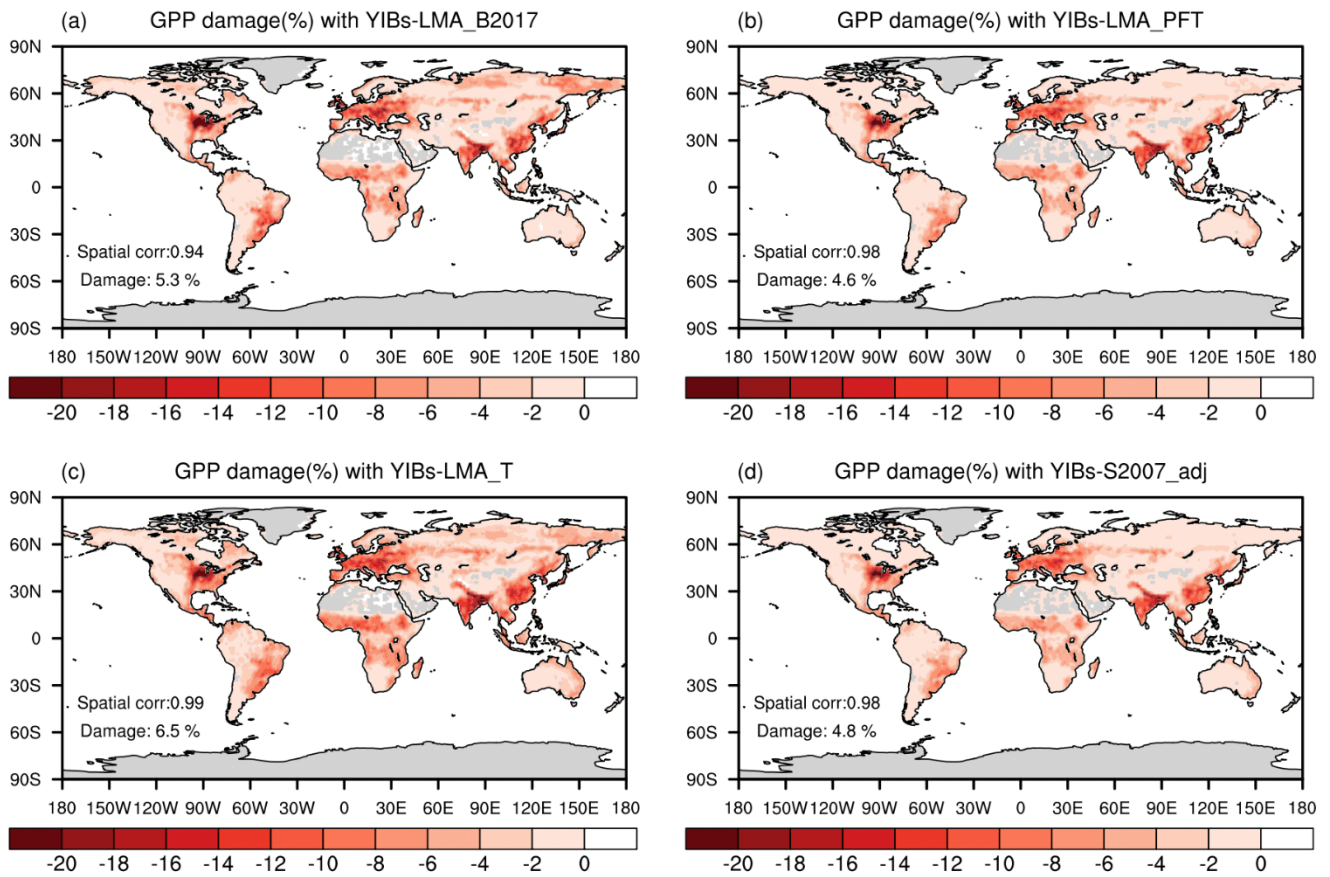


762

763 **Figure 45.** Global O<sub>3</sub> vegetation damage simulated with the LMA-based scheme. Results shown are the  
 764 (a) GPP reduction percentages by O<sub>3</sub> simulated with the YIBs-LMA framework (gridded LMA from  
 765 M2018,  $x=0.019 \text{ nmol g}^{-1} \text{ s}^{-1}$ , and  $a=3.5 \text{ nmol}^{-1} \text{ s g}$ ), and (b) their differences compared to the predictions  
 766 from YIBs-S2007\_adj simulation. Blue (red) patches indicate the regions where damages predicted in  
 767 YIBs-LMA are lower (higher) than those in YIBs-S2007\_adj.

768

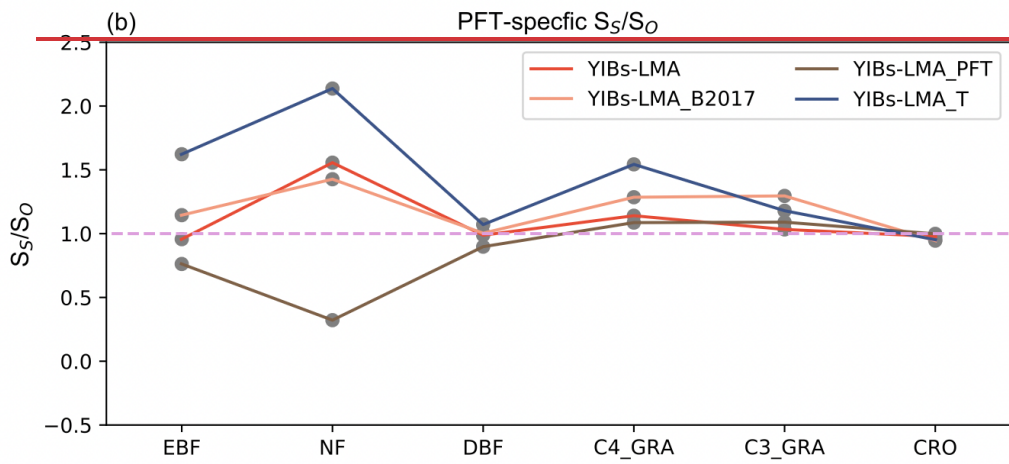
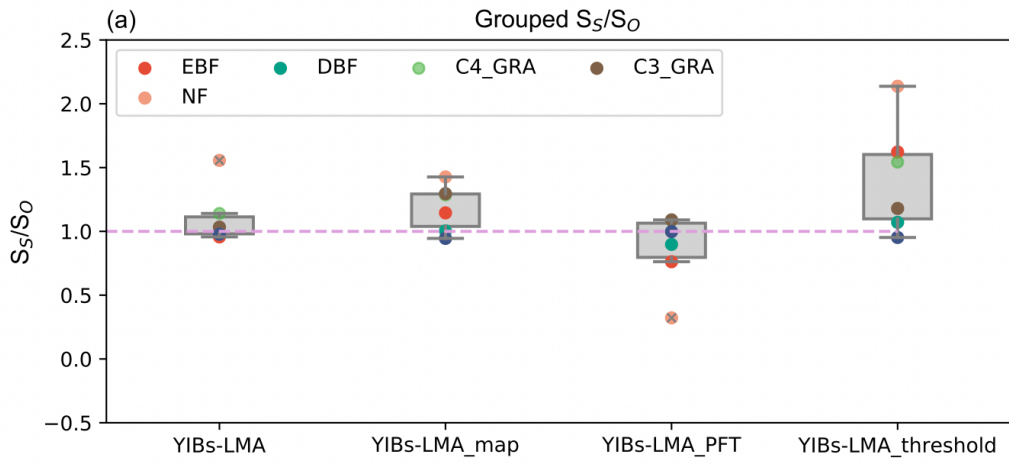




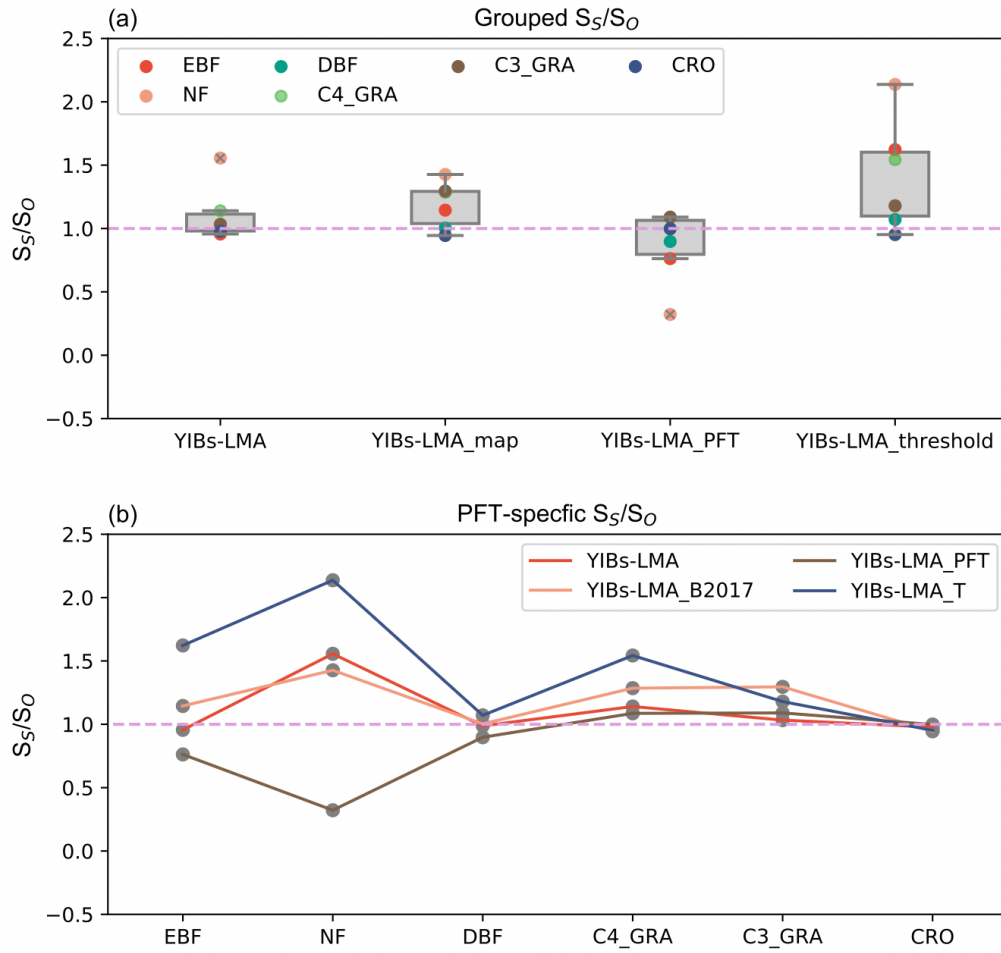
770

771 **Figure 56.** Global O<sub>3</sub>-induced GPP reductions simulated in four supporting experiments. All damage  
 772 maps are based on optimal parameters shown in Table 1. The spatial correlation coefficients between  
 773 YIBs-LMA and these supporting simulations are shown on each panel as well as the global average  
 774 damage percentage of each map. Simulations are described in Table 1.

775



776



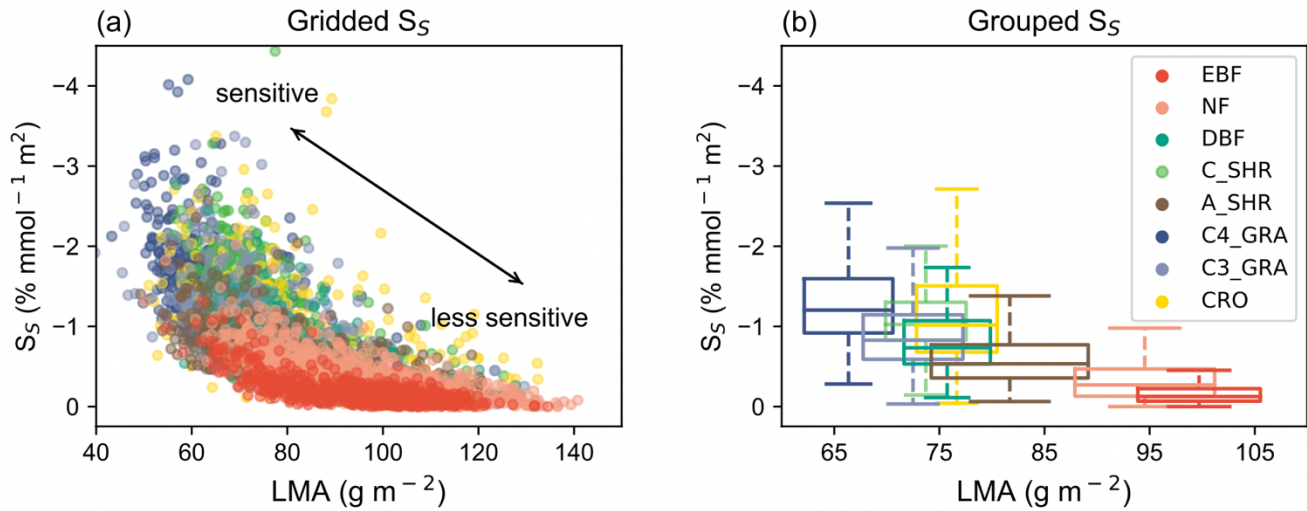
777

778 **Figure 67.** Comparison of  $S_5/S_0$  among supporting experiments. Individual ratios for (b) different PFTs  
 779 are grouped to the boxplot in (a). All experiments adopt optimal parameters shown in Table 1.

780



781



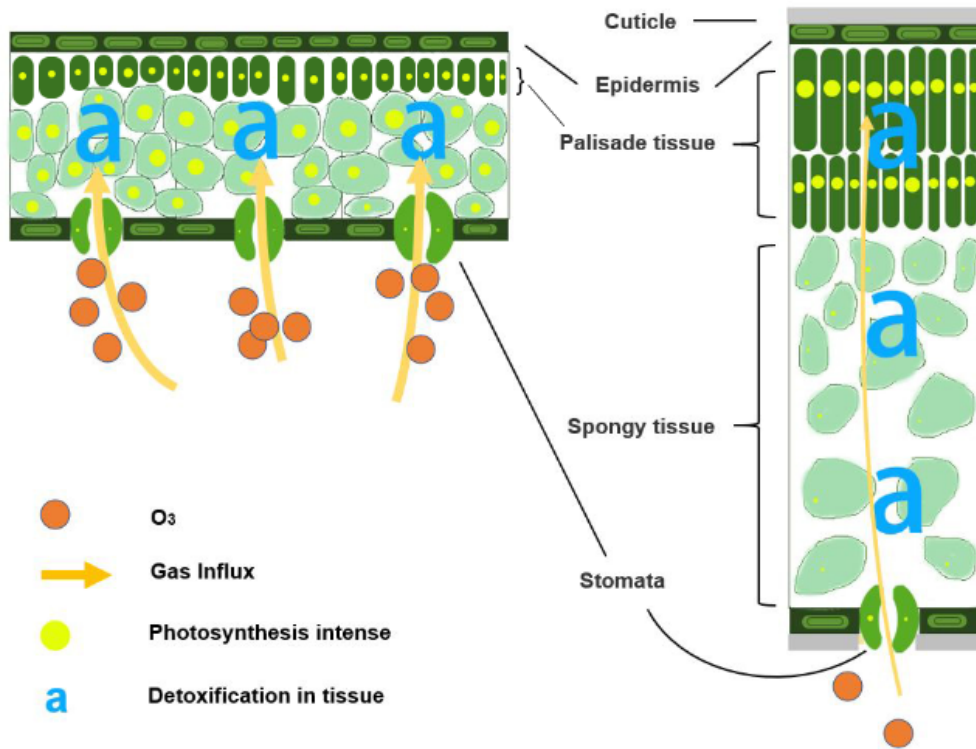
782

783 **Figure 78.** Relationships between O<sub>3</sub> sensitivity and LMA. (a) Simulated O<sub>3</sub> sensitivity ( $S_5$ ) at each grid  
 784 is compared with LMA for different PFTs. Gridded  $S_5$  is derived as GPP change per unit  $\text{POD}_{y=1}$  from  
 785 the YIBs-LMA simulation. Each point represents the value in a grid cell with a dominant PFT. (b) The  
 786 PFT-level relationships between LMA and O<sub>3</sub> sensitivity are grouped as boxplots, which indicate the  
 787 median, 25<sup>th</sup> percentile, and 75<sup>th</sup> percentile of y-axis variables within the same PFT. The width of boxplots  
 788 represents one standard deviation of LMA for a specific PFT.

789

Mode1 : Sensitive, Fast

Mode 2 : Less-sensitive, Slow



790

791 **Figure 89.** Illustration of the relationships between leaf trade-off strategy and its sensitivity to  $O_3$

792